

Numerical Challenges for Resolving Spike Dynamics for Two One-Dimensional Reaction-Diffusion Systems

Wentao Sun*, Tao Tang[†], Michael J. Ward[‡], Juncheng Wei[§]

Abstract

Asymptotic and numerical methods are used to highlight different types of dynamical behaviors that occur for the motion of a localized spike-type solution to the singularly perturbed Gierer-Meinhardt and Schnakenburg reaction-diffusion models in a one-dimensional spatial domain. Depending on the parameter range in these models, there can either be a slow evolution of a spike towards the midpoint of the domain, a sudden oscillatory instability triggered by a Hopf bifurcation leading to an intricate temporal oscillation in the height of the spike, or a pulse-splitting instability leading to the creation of new spikes in the domain. Criteria for the onset of these oscillatory and pulse-splitting instabilities are obtained through asymptotic and numerical techniques. A moving-mesh numerical method is introduced to compute these different behaviors numerically, and results are compared with corresponding results computed using a method of lines based software package.

1 Introduction

Since the pioneering work of Turing [27], there have been many studies of instabilities of spatially homogeneous patterns in two-component reaction-diffusion systems. The criterion for the onset of instabilities of these spatially homogeneous patterns, and the associated weakly nonlinear theory describing the evolution of small disturbances, has largely been explored. However, in the singularly perturbed limit, many reaction-diffusion systems can give rise to spike-type patterns whereby one of the components of the system becomes spatially localized at certain points in the domain. In different contexts, these types of solutions are also referred to as pulses (cf. [5]) or spots (cf. [16]). In contrast to spatially homogeneous solutions, the instabilities and the dynamics of these localized patterns is not nearly as well understood. In this paper, we use asymptotic and numerical methods to highlight different types of dynamical behaviors and instabilities that occur for the motion of

*Mathematics and System Science School of Shandong University, Jinan, 250100, Shandong, P.R. China

[†]Department of Mathematics, The Hong Kong Baptist University, Kowloon Tong, Hong Kong

[‡]Department of Mathematics, U. B. C, Vancouver, Canada V6T 1Z2; (corresponding author)

[§]Department of Mathematics, Chinese University of Hong Kong, New Territories, Hong Kong

a localized spike-type solution to the singularly perturbed Gierer-Meinhardt and Schnakenburg reaction-diffusion models in a one-dimensional spatial domain.

The Gierer-Meinhardt (GM) model, introduced in [9], is a reaction-diffusion system of activator-inhibitor type. It has been widely used to model localization processes in nature, such as cell differentiation and morphogenesis (cf. [10]), biological pattern formation (cf. [15]), and the formation of sea-shell patterns (cf. [16]). In dimensionless form, the GM model can be written as

$$a_t = \varepsilon^2 a_{xx} - a + \frac{a^p}{h^q}, \quad -1 < x < 1, \quad t > 0, \quad (1.1a)$$

$$\tau h_t = D h_{xx} - h + \varepsilon^{-1} \frac{a^m}{h^s}, \quad -1 < x < 1, \quad t > 0, \quad (1.1b)$$

$$a_x(\pm 1, t) = h_x(\pm 1, t) = 0; \quad a(x, 0) = a_0(x), \quad h(x, 0) = h_0(x). \quad (1.1c)$$

Here a , h , $0 < \varepsilon \ll 1$, $D > 0$, and $\tau \geq 0$, represent the activator concentration, inhibitor concentration, activator diffusivity, inhibitor diffusivity, and reaction-time constant, respectively. The parameters D and τ are assumed to be constant. The usual assumption on the exponents (p, q, m, s) (cf. [9]) are that they satisfy

$$p > 1, \quad q > 0, \quad m > 1, \quad s \geq 0, \quad \text{with} \quad \zeta \equiv \frac{qm}{(p-1)} - (s+1) > 0. \quad (1.2)$$

A typical exponent set is $(p, q, m, s) = (2, 1, 2, 0)$. The nondimensionalization of the dimensional GM model, which results in (1.1), is summarized in Appendix A.

The Schnakenburg model [26] is another well-known two-component reaction-diffusion system. In the absence of diffusion, the kinetics for this model are such that spatially homogeneous patterns can exhibit Hopf bifurcations leading to temporal oscillations. When the ratio of the diffusion coefficients in the model is suitably large, spike-type solutions to this model are also possible (cf. [29], [13]). In this limit, and with the nondimensionalization procedure summarized in Appendix A, the Schnakenburg model can be written in dimensionless variables as

$$u_t = \varepsilon^2 u_{xx} - u + v u^2, \quad -1 < x < 1, \quad t > 0, \quad (1.3a)$$

$$\tau v_t = D v_{xx} + \frac{1}{2} - \varepsilon^{-1} v u^2, \quad -1 < x < 1, \quad t > 0, \quad (1.3b)$$

$$u_x(\pm 1, t) = v_x(\pm 1, t) = 0; \quad u(x, 0) = u_0(x), \quad v(x, 0) = v_0(x). \quad (1.3c)$$

For the case $\tau = 0$, there have been several recent studies of the stability of equilibrium spike-type solutions to the GM model (1.1) and the Schnakenburg model (1.3). The stability of symmetric multi-spike equilibria and the existence and stability of asymmetric multi-spike equilibria for the GM model have been analyzed using formal asymptotic techniques in [12] and [28], respectively. A rigorous framework for these stability analyses is given in [33]. Similar results for the existence

and stability of symmetric and asymmetric multi-spike equilibria for (1.3) when $\tau = 0$ have been obtained in [13] and [29].

There are only a few stability results for the case where $\tau > 0$. The difficulty with the analysis in this case is that oscillatory instabilities may emerge for certain ranges of τ . This was anticipated in [19] where numerical results were shown at two different values of τ for the oscillatory motion of a boundary spike for the shadow GM model obtained by taking the limit $D \rightarrow \infty$ in (1.1). For $\tau > 0$, and D sufficiently large, the stability of a one-spike solution to (1.1) was analyzed rigorously in [20] under the condition that the exponents (p, q, m, s) in the model are such that $\zeta \rightarrow 0^+$ in (1.2). For the shadow GM model, a combination of rigorous and formal asymptotic and numerical techniques were used in [30] to determine the conditions for the onset of oscillatory stabilities of an equilibrium one-spike solution to the shadow GM model in N spatial dimensions.

For the case $\tau = 0$ and $D = O(1)$, the dynamics of a collection of spikes for the GM model has been analyzed in [11] by deriving equations of motion for the slow evolution of the centers of the spikes. It was shown asymptotically and numerically in [11] that a collection of spikes will move slowly in time, but can experience a sudden instability whereby one of the spikes collapses monotonically to zero on an $O(1)$ time scale. The stability and dynamics of spike solutions with $\tau > 0$ and $D = O(1)$ has not been considered previously.

There are two main purposes of this paper. The first goal is to highlight the different types of behaviors associated with the dynamics of a localized spike-type solution for (1.1) and (1.3). Two key parameters in the analysis are the reaction-time constant τ and the diffusivity D . Asymptotic methods are used as a guide to provide a partial analysis of the range of behaviors seen. For the case $\tau = 0$, there will be a slow evolution of the center of the spike towards the midpoint of the domain. The motion occurs on a long time-scale of order $O(\varepsilon^{-2})$. An asymptotic differential equation for the motion of the center of the spike is derived. For other ranges of the parameter τ , a spike can move slowly in the domain, but then at some point during the slow evolution develop a sudden and very intricate oscillatory motion in its height that occurs on an $O(1)$ time-scale. This type of oscillatory instability, which is initially triggered through a Hopf bifurcation, has not been observed previously. By deriving a nonlocal eigenvalue problem, and then by studying this problem numerically, we show that this instability will occur when $\tau > \tau_0$, where τ_0 depends on D and on the location, x_0 , of the spike at a given time. The values for τ_0 are computed numerically for (1.1) and (1.3). For other ranges of the parameters, a pulse-splitting instability can occur for (1.1), and for a certain generalized form of the basic model (1.1). Although we do not give a detailed account of pulse-splitting instabilities for (1.1), we give a prediction for the critical value of D below which pulse-splitting instabilities occur. For the well-known Gray-Scott model, pulse-splitting instabilities and traveling waves have been explored in considerable detail in [25], [5], [6], [7], [8], [17], [22] (see also the references therein). They were also predicted to occur for the GM model when D in (1.1b) is sufficiently small (cf. [21]).

These various dynamical behaviors of spike motion highlight potential challenges associated with the numerical solution to (1.1) and (1.3) using only a moderate number of spatial meshpoints. There are several key challenges. Since a spike is localized in space, there is a need for a fine spatial

grid near the core of the spike. This spatial grid needs to adapt to the slow change in the location of the spike as it moves across the domain. In addition, since a spike can exhibit a fast oscillatory instability in its height, an accurate long-time integration is needed in order to capture the slow drift of the center of the spike in the presence of an $O(1)$ time-scale oscillation of the height of the spike. Pulse-splitting instabilities, whereby new spikes are created, provide a severe challenge as they require that new computational meshpoints be generated to follow each new spike. In our one-dimensional spatial domain it is possible to largely overcome these difficulties by using a very large number of equidistantly spaced spatial meshpoints and stringent tolerances on the adaptive time stepping control for a method of lines based PDE solver from the NAG library [18]. Although, this type of brute force approach is possible in one space dimension, it is computationally inefficient and, from practical purposes, infeasible in more than one space dimension, where similar types of dynamical behavior for spike solutions is likely to occur. In this light, the second goal of this paper is to introduce a moving-mesh numerical method to compute a spike-type solution for (1.1) and (1.3) using only a moderate number of meshpoints. Numerical results from this moving-mesh method and from a software routine in the NAG library are shown. Work is in progress to extend the moving-mesh method to two space dimensions in the future. A different type of moving-mesh method, described in [3], has been used previously for the Gray-Scott model in [5].

The outline of this paper is as follows. In §2 we introduce a moving-mesh numerical method for computing a spike-type solution for (1.1) and (1.3). In §3, for the case $\tau = 0$ in (1.1) and (1.3), we study both asymptotically and numerically the slow, regular, motion of a spike towards the midpoint of the domain. In §4, asymptotic analysis is used to determine the conditions on τ for which an oscillatory instability in the height of the spike is triggered. Numerical computations are shown for values of τ both near, and well beyond, this critical value. These computations highlight the various types of oscillatory instabilities. In §5 and §6 pulse-splitting instabilities are shown for (1.1) and for a generalization of (1.1).

2 The Moving Mesh Method

In this section, we describe the moving mesh numerical method used to approximate the solution to (1.1). A similar discretization scheme is used to compute solutions to (1.3).

Let $-1 = x_0 < x_1 < \dots < x_N = 1$ be a partition of $[-1, 1]$. A natural way to discretize (1.1) is to use the central differencing in space to handle the diffusion terms and to use a method of line approach to deal with the time derivatives. One of the difficult issues is how to handle the boundary conditions. There are several ways to deal with the nonreflecting boundary conditions in (1.1c). For example, by using Taylor expansions with the given boundary conditions we can determine numerically the boundary values at $x = \pm 1$. Then the method of line equations are set up at $x = x_1, \dots, x_{N-1}$. However, our numerical experiments have shown that this approach in general leads to wrong solutions: in most cases the numerical solutions for the activator concentration diffuse to zero at a finite time.

It is found that an appropriate numerical scheme for the GM model (1.1) has to satisfy the two compatibility conditions

$$\int_{-1}^1 a_t dx + \int_{-1}^1 a dx = \int_{-1}^1 \frac{a^p}{h^q} dx, \quad (2.1a)$$

$$\tau \int_{-1}^1 h_t dx + \int_{-1}^1 h dx = \varepsilon^{-1} \int_{-1}^1 \frac{a^m}{h^s} dx. \quad (2.1b)$$

With this in mind, we propose the following numerical scheme for solving (1.1). Let the approximations to the activator and inhibitor concentrations at the grid point x_i be defined by $\{A(t)_i\}_0^N$ and $\{H(t)_i\}_0^N$, respectively. On a nonuniform mesh, we introduce the discretizations

$$\delta_{\hat{x}}(\delta_x A(t))_i = \frac{2}{x_{i+1} - x_{i-1}} \left(\frac{A(t)_{i+1} - A(t)_i}{x_{i+1} - x_i} - \frac{A(t)_i - A(t)_{i-1}}{x_i - x_{i-1}} \right), \quad i = 1, \dots, N-1, \quad (2.2a)$$

$$\delta_{\hat{x}}(\delta_x A(t))_0 = \frac{A(t)_1 - A(t)_0}{(x_1 - x_0)^2}, \quad \delta_{\hat{x}}(\delta_x A(t))_N = \frac{A(t)_{N-1} - A(t)_N}{(x_N - x_{N-1})^2}. \quad (2.2b)$$

The approximate solutions $A(t)$ and $H(t)$ are made to satisfy the following semi-discrete equations, for $i = 0, \dots, N$ and $t > 0$:

$$(A(t)_i)_t = \varepsilon^2 \delta_{\hat{x}}(\delta_x A(t))_i - A(t)_i + \frac{A(t)_i^p}{H(t)_i^q}, \quad (2.3a)$$

$$\tau (H(t)_i)_t = D \delta_{\hat{x}}(\delta_x H(t))_i - H(t)_i + \varepsilon^{-1} \frac{A(t)_i^m}{H(t)_i^s}, \quad (2.3b)$$

$$A(0)_i = a_0(x_i), \quad H(0)_i = h_0(x_i). \quad (2.3c)$$

We now generate the moving mesh based on the equidistribution principle in one dimension as introduced by de Boor [4]. Let $x \in [-1, 1]$ and $\xi \in [0, 1]$ denote the physical and computational coordinates, respectively. The mesh $x(\xi)$ is defined in terms of a differentiable mesh transformation from $[0, 1]$ to $[-1, 1]$. The underlying strategy for determining $x(\xi)$ is to require equidistribution of a positive monitor function, say $M(a, a_x)$, so that

$$\int_0^x M dy = \xi \int_0^1 M dy, \quad \xi \in [0, 1]; \quad x(0) = -1, \quad x(1) = 1. \quad (2.4)$$

The above integral form was proposed in [34].

Roughly speaking, the role of the monitor function is to cluster more grid points in the regions where the monitor has the largest values. A popular class of monitor function depends on the gradient of the physical solution to be adapted, see, e.g., [2]. However, for problems with finitely many peaks, a typical choice for the monitor function (cf. [14], [24]) is

$$M(a(x, t)) = \sqrt{1 + ca^2(x, t)}, \quad (2.5)$$

where $c > 0$ is a user-prescribed parameter, chosen depending on the character of the physical solution. In the computations below we take M as given in (2.5) with $c = 1$.

Suppose that a uniform mesh is given to the computational domain by $\{\xi_i\}_0^N$. We denote the corresponding mesh in x by $\{x_i\}_0^N$. For a chosen monitor function $M(a(x, t))$, the equidistribution principle (2.4) can be expressed in the discrete form:

$$\int_{x_i}^{x_{i+1}} M(a(y, t)) dy = \int_{x_{i-1}}^{x_i} M(a(y, t)) dy, \quad i = 1, \dots, N - 1. \quad (2.6)$$

Using the mid-point rule leads to the following system:

$$M(a(x_{i+1/2}, t))(x_{i+1} - x_i) = M(a(x_{i-1/2}, t))(x_i - x_{i-1}), \quad i = 1, \dots, N - 1, \quad (2.7)$$

with $x_0 = -1$ and $x_N = 1$.

We now describe the procedure for solving the semi-discrete system (2.3). From the initial condition a_0 we first generate the initial adaptive mesh by solving the linear system (2.7) – in this case the monitor function is given explicitly. We then map the initial value of the activator and inhibitor concentrations to the initial adaptive mesh at $t = 0$. Then, once the approximate solution $\{A_i, H_i\}_0^N$ on the adaptive moving mesh is known at $t = t_n > 0$, the activator concentration and inhibitor concentrations are then computed at $t = t_{n+1}$ by means of an explicit fourth order Runge Kutta method on the mesh $\{x_i(t_n)\}_0^N$. This high order time integration scheme is needed to capture oscillatory instabilities. We generate the mesh at next time step by solving the linearized system (2.7) with $M_{i+1/2}$ and $M_{i-1/2}$ computed by the value of $A(t_n)$. We then map the activator concentration $A(t_{n+1})$ on the previous mesh to the present mesh by using first order linear interpolation. In the special case where $\tau = 0$ in (2.3b) we first compute $H(t_{n+1})$ on the present mesh from the solution to (2.3b) using the known values of $A(t_{n+1})$.

3 The Dynamics with a Zero Reaction-Time Constant

In this section we consider the evolution of a one-spike solution to the GM model (1.1) and the Schnakenburg model (1.3) when $\tau = 0$. For the case $\tau = 0$, the dynamics of a one-spike solution to (1.1) for $\varepsilon \ll 1$ was analyzed in [12]. In §3.2 we derive an analogous result for the dynamics of a one-spike solution to (1.3). The asymptotic results for the location of the spike as a function of time are compared with corresponding numerical results computed using the moving-mesh method of §2 and the NAG library routine D03PCF [18].

3.1 The GM Model

For $\varepsilon \ll 1$, the method of matched asymptotic expansions was used in [12] to derive the following asymptotic result for the dynamics of a one-spike solution to (1.1):

Proposition 3.1 (From [12]): For $0 < \varepsilon \ll 1$ and $\tau = 0$, the dynamics of a one-spike solution to (1.1) is characterized by

$$a(x, t) \sim a_c \equiv H^\gamma w(\varepsilon^{-1}[x - x_0(t)]), \quad (3.1a)$$

$$h(x, t) \sim h_c \equiv HG_m[x; x_0(t)]/G_m[x_0(t); x_0(t)], \quad (3.1b)$$

where $\gamma \equiv q/(p-1)$, and the spike location $x_0(t)$ satisfies the differential equation

$$\frac{dx_0}{dt} \sim -\frac{\varepsilon^2 q}{(p-1)\sqrt{D}} \left(\tanh \left[D^{-1/2}(1+x_0) \right] - \tanh \left[D^{-1/2}(1-x_0) \right] \right). \quad (3.1c)$$

Here $w(y)$ is the unique, positive, solution to

$$w'' - w + w^p = 0, \quad -\infty < y < \infty; \quad w \rightarrow 0 \quad \text{as} \quad |y| \rightarrow \infty; \quad w'(0) = 0, \quad w(0) > 0. \quad (3.1d)$$

In (3.1b), $G_m(x; x_0)$ is the Green's function satisfying

$$DG_{mxx} - G_m = -\delta(x - x_0), \quad -1 < x < 1; \quad G_{mx}(\pm 1; x_0) = 0, \quad (3.1e)$$

and the constant $H(t)$ is defined in terms of G_m by

$$H \equiv \left[\frac{1}{b_m G_m(x_0; x_0)} \right]^{1/\zeta}, \quad b_m \equiv \int_{-\infty}^{\infty} [w(y)]^m dy, \quad (3.1f)$$

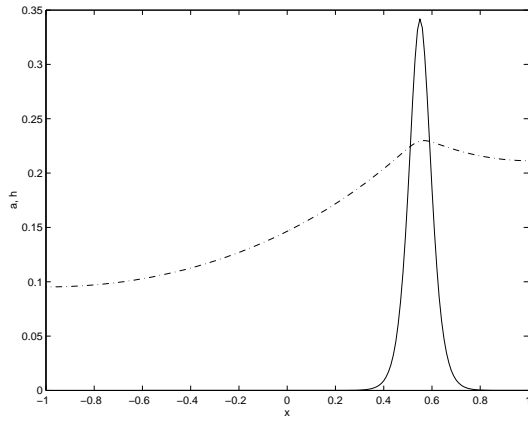
where ζ is defined in (1.2).

Experiment 1: To illustrate the moving-mesh method for solving (1.1), we take $\varepsilon = 0.03$, $D = 1$, $\tau = 0$, and the exponent set $(p, q, m, s) = (2, 1, 2, 0)$. We take the spike to be located at $x = 0.6$ initially. The initial profiles for a and h are chosen to have the form in (3.1a) and (3.1b) respectively, so that

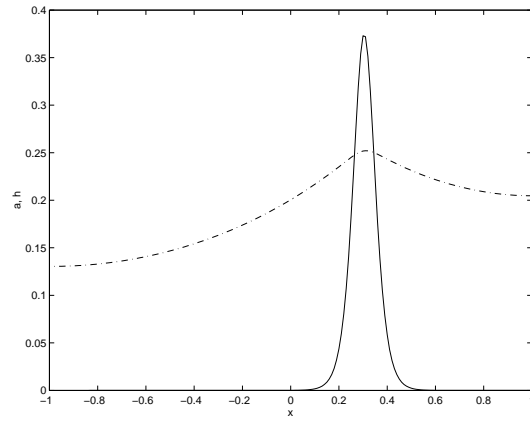
$$a_0(x) = \frac{3H}{2} \operatorname{sech}^2 \left(\frac{\varepsilon^{-1}}{2} [x - x_0(0)] \right), \quad H = [6G_m(x_0; x_0)]^{-1}, \quad (3.2)$$

with $x_0(0) = 0.6$.

In Fig. 1–2, we plot the numerical solution to (1.1) based on our moving-mesh method with $N = 100$ meshpoints. In Table 1 we compare the asymptotic and numerical results for $x_0(t)$ with the moving-mesh results for $N = 100$ and $N = 200$ meshpoints. The asymptotic result is obtained by integrating (3.1c) with $x_0(0) = 0.6$. To compare with these results, we solve (1.1) for this parameter set using the NAG library code D03PCF [18] with $N = 2000$ equally spaced meshpoints and strict tolerances on the time-stepping. The results, which should be very close to the true solution, are shown in the fourth column of Table 1. Notice that the moving-mesh method with $N = 200$ gives a rather close approximation to the results from the NAG routine.

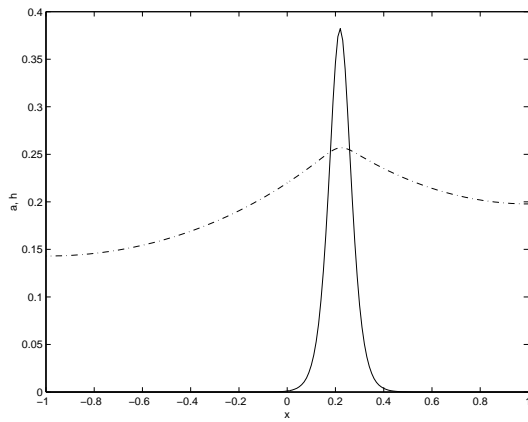


(a) a at $t = 100$

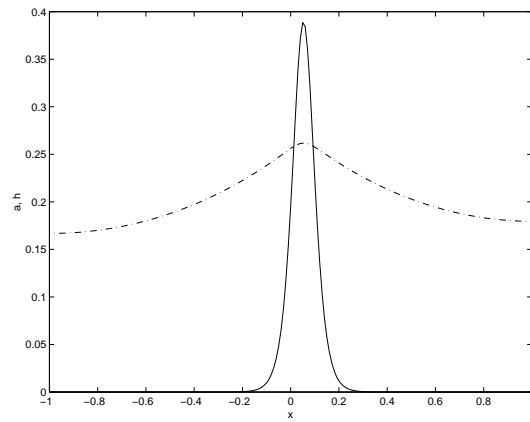


(b) a and h at $t = 800$

Figure 1: Plots of a (solid curve) and h (dashed curve) at different times.



(a) a and h at $t = 1200$



(b) a and h at $t = 3000$

Figure 2: Plots of a (solid curve) and h (dashed curve) at different times.

t	$x_0(t)$ (ASY)	$x_0(t)$ (MM, N=200)	$x_0(t)$ (MM, N=100)	$x_0(t)$ (NAG)
100	0.55338	0.555	0.55	0.5506
400	0.43577	0.425	0.43	0.4272
800	0.31891	0.305	0.33	0.3064
1200	0.23441	0.215	0.23	0.2207
1800	0.14834	0.135	0.015	0.1353
3000	0.05975	0.055	0.07	0.0512

Table 1: Comparison of the asymptotic and numerical results for the center $x_0(t)$ of the spike for Experiment 1. Here N is the number of mesh points and (MM) denotes moving-mesh.

3.2 The Schnakenberg Model

We now consider the evolution of a one-spike solution for (1.3). The adaptive moving-mesh numerical method for this problem is similar to that described in §2 for the GM model. To compare with results from the numerical method, we use the method of matched asymptotic expansions for $\varepsilon \ll 1$ to derive a differential equation for the center of a spike for a one-spike solution to (1.3). We obtain the following result:

Proposition 3.2: *For $0 < \varepsilon \ll 1$ and $\tau = 0$, the dynamics of a one-spike solution to (1.3) is characterized by*

$$u(x, t) \sim u_c \equiv V^{-1} w(\varepsilon^{-1}[x - x_0(t)]) , \quad (3.3a)$$

$$v(x, t) \sim v_c \equiv G_s[x; x_0(t)] - G_s[x_0(t); x_0(t)] + V . \quad (3.3b)$$

Here w is the solution to (3.1d) with $p = 2$. The spike location $x_0(t)$ and the constant V satisfy

$$\frac{dx_0}{dt} \sim - \left(\frac{\varepsilon^2}{6D} \right) x_0 , \quad V = b_2 , \quad (3.3c)$$

where b_m is defined in (3.1f). In (3.3b), $G_s(x; x_0)$ is the modified Green's function satisfying

$$DG_{sxx} + \frac{1}{2} = -\delta(x - x_0) , \quad |x| \leq 1 ; \quad G_{sx}(\pm 1; x_0) = 0 ; \quad \int_{-1}^1 G_s(x; x_0) dx = 0 . \quad (3.3d)$$

It can be calculated explicitly as

$$G_s(x; x_0) = -\frac{1}{4D}(x^2 + x_0^2) + \frac{1}{2D}|x - x_0| - \frac{1}{6D} . \quad (3.3e)$$

We now derive the result (3.3) using the method of matched asymptotic expansions. In the analysis two expansions are needed: an inner expansion near the core of the spike and an outer expansion away from the core. In the inner region, near $x = x_0$, we introduce new variables by

$$y = \varepsilon^{-1} [x - x_0(\tau)], \quad \tilde{v}(y) = v(x_0 + \varepsilon y), \quad \tilde{u}(y) = u(x_0 + \varepsilon y), \quad \tau = \varepsilon^2 t, \quad (3.4a)$$

and we expand

$$\tilde{v}(y) = \tilde{v}_0(y) + \varepsilon \tilde{v}_1(y) + \dots, \quad \tilde{u}(y) = \tilde{u}_0(y) + \varepsilon \tilde{u}_1(y) + \dots. \quad (3.4b)$$

We substitute (3.4) into (1.3) and collect powers of ε . The leading order problem, on $-\infty < y < \infty$, is

$$\tilde{u}_0'' - \tilde{u}_0 + \tilde{v}_0 \tilde{u}_0^2 = 0; \quad \tilde{v}_0'' = 0. \quad (3.5)$$

The solution is

$$\tilde{u}_0(y) = V^{-1} w(y), \quad w(y) \equiv \frac{3}{2} \operatorname{sech}^2\left(\frac{y}{2}\right), \quad \tilde{v}_0 = V. \quad (3.6)$$

Here $w(y)$ is the solution to (3.1d) when $p = 2$, and $V = V(\tau)$ is a function to be determined. At next order, we obtain that \tilde{u}_1 and \tilde{v}_1 satisfy

$$\tilde{u}_1'' - \tilde{u}_1 + 2w\tilde{u}_1 = -\frac{w^2}{V}\tilde{v}_1 - x_0' \frac{w'}{V}, \quad -\infty < y < \infty, \quad (3.7a)$$

$$D\tilde{v}_1'' = \frac{1}{V}w^2, \quad -\infty < y < \infty, \quad (3.7b)$$

with $\tilde{u}_1 \rightarrow 0$ exponentially as $|y| \rightarrow \infty$. In (3.7a), $x_0' \equiv dx_0/d\tau$. The right-hand side of (3.7a) must be orthogonal to the solution w' of the homogeneous problem for (3.7a). From this solvability condition, we obtain

$$x_0' = -\frac{\int_{-\infty}^{\infty} w^2 w' \tilde{v}_1 dy}{V \int_{-\infty}^{\infty} [w']^2 dy}. \quad (3.8)$$

If we integrate (3.8) by parts twice, and use the facts that \tilde{v}_1'' and w are even functions, we get

$$x_0' = \frac{1}{6V} \left(\frac{\int_{-\infty}^{\infty} [w(y)]^3 dy}{\int_{-\infty}^{\infty} [w'(y)]^2 dy} \right) \left[\lim_{y \rightarrow +\infty} \tilde{v}_1' + \lim_{y \rightarrow -\infty} \tilde{v}_1' \right]. \quad (3.9)$$

In the outer region away from the core of the spike, u is exponentially small and $v = O(1)$. We thus expand $v = v_0 + \dots$, where v_0 satisfies

$$Dv_0'' + \frac{1}{2} - \varepsilon^{-1} v_0 u^2 = 0, \quad -1 < x < 1; \quad v_0'(\pm 1) = 0. \quad (3.10)$$

Since u is localized near $x = x_0$, the ε^{-1} term in (3.10) can be approximated as a Dirac mass. This gives

$$Dv_0'' + \frac{1}{2} - \frac{b_2}{V}\delta(x - x_0) = 0, \quad -1 < x < 1; \quad v_0'(\pm 1) = 0, \quad (3.11)$$

where b_2 is defined in (3.1f). The problem (3.11) must satisfy a solvability condition, as seen by integrating the differential equation in (3.11) across the interval $-1 < x < 1$. This condition yields that

$$V = b_2 \equiv \int_{-\infty}^{\infty} [w(y)]^2 dy. \quad (3.12)$$

With $w(y)$ as in (3.6), we calculate that $V = 6$. The solution to (3.11) is

$$v_0(x) = G_s(x; x_0) + \bar{v}, \quad (3.13)$$

where \bar{v} is a constant to be found, and G_s is the modified Green's function satisfying (3.3d). The solution to (3.3d) is simply (3.3e).

Next, we match the inner and outer solutions. This requires that

$$v_0(x_0) = V = 6, \quad \text{and} \quad \lim_{y \rightarrow +\infty} \tilde{v}'_1 + \lim_{y \rightarrow -\infty} \tilde{v}'_1 = v_{0x}(x_{0+}) + v_{0x}(x_{0-}). \quad (3.14)$$

Thus, setting $v_0(x_0) = 6$ in (3.13), we obtain that $\bar{v} = -G_s(x_0; x_0) + 6$. Substituting \bar{v} into (3.13) we obtain (3.3b) above. Finally, we substitute (3.3b) into the second equation of (3.14). Then, from (3.9), we obtain a differential equation for the spike location

$$\frac{dx_0}{d\tau} \sim \frac{1}{36} \left(\frac{\int_{-\infty}^{\infty} [w(y)]^3 dy}{\int_{-\infty}^{\infty} [w'(y)]^2 dy} \right) [G_{sx}(x_0^+; x_0) + G_{sx}(x_0^-; x_0)]. \quad (3.15)$$

Using (3.3e) for G_s , $\tau = \varepsilon^2 t$, and the form for w in (3.6) to calculate the ratio of the two integrals in (3.15), we obtain the result (3.3c) for the dynamics of a one-spike solution to (1.3). This completes the derivation of proposition 3.2.

Experiment 2: We take $\tau = 0$, $\varepsilon = 0.03$, and $D = 1.0$ in (1.3). We take the initial location of the spike to be $x_0(0) = 0.25$. The initial profiles for u and v are as given in (3.3a) and (3.3b), respectively. In Fig. 3, we plot the numerical solution to (1.3) at three different times computed using our moving-mesh method with $N = 200$ meshpoints. In Table 2 we compare the asymptotic and numerical results for $x_0(t)$ with the moving-mesh results for $N = 200$ meshpoints. The asymptotic result is obtained by integrating (3.3c) with $x_0(0) = 0.25$. In the fourth column we again show the results obtained using the NAG library code D03PCF [18] with $N = 2000$ meshpoints and strict tolerances on the time-stepping. For this example, the asymptotic result is very close to the values computed from the NAG routine. The moving-mesh method with $N = 200$ meshpoints also performs well.

t	$x_0(t)$ (ASY)	$x_0(t)$ (MM, N=200)	$x_0(t)$ (NAG)
204	0.242466	0.2412	0.2425
486	0.232423	0.2311	0.2324
864	0.219612	0.2206	0.2196
1314	0.205277	0.2011	0.2053
1884	0.188455	0.1812	0.1885
2274	0.177746	0.1710	0.1778

Table 2: Comparison of the asymptotic and numerical results for the center $x_0(t)$ of the spike for Experiment 2. Here N is the number of mesh points and (MM) denotes moving-mesh.

4 Oscillatory Dynamics with a Nonzero Reaction-Time Constant

In this section we study the stability, on an $O(1)$ time-scale, of one-spike quasi-equilibrium profiles for the GM and Schnakenburg models with respect to a nonzero reaction-time constant $\tau > 0$. The spike is assumed to be located initially at some point $x_0 \in (-1, 1)$. In §4.1 we formulate nonlocal eigenvalue problems that determine the stability of these profiles for (1.1) and for (1.3). From a numerical computation of these eigenvalue problems, in §4.2 we give some results for the critical value of τ at which an oscillatory instability is triggered. This critical value of τ depends on x_0 and on D . In §4.3 and §4.4 we give some full numerical results for (1.1) and (1.3) showing oscillatory instabilities for a spike at the origin and for a slowly drifting spike, respectively.

4.1 The Nonlocal Eigenvalue Problems

We first formulate a nonlocal eigenvalue problem that determines the stability on an $O(1)$ time scale of the quasi-equilibrium profile for the GM model (1.1).

For a fixed $x_0 \in (-1, 1)$, the quasi-equilibrium profile a_c, h_c for the GM model is defined in (3.1). To study the stability of this profile, we let $a = a_c + e^{\lambda t}\phi$, $h = h_c + e^{\lambda t}\eta$, where $\phi \ll 1$ and $\eta \ll 1$. Substituting into (1.1), we obtain the eigenvalue problem

$$\varepsilon^2 \phi_{xx} - \phi + \frac{pa_c^{p-1}}{h_c^q} \phi - \frac{qa_c^p}{h_c^{q+1}} \eta = \lambda \phi, \quad -1 < x < 1, \quad (4.1a)$$

$$D\eta_{xx} - (1 + \tau\lambda)\eta = -\varepsilon^{-1} \frac{ma_c^{m-1}}{h_c^s} \phi + \varepsilon^{-1} \frac{sa_c^m}{h_c^{s+1}} \eta, \quad -1 < x < 1, \quad (4.1b)$$

$$\phi_x(\pm 1) = \eta_x(\pm 1) = 0. \quad (4.1c)$$

We look for eigenvalues of (4.1) that are $O(1)$ as $\varepsilon \rightarrow 0$. The corresponding eigenfunction is localized, and has the form

$$\phi(x) \sim \Phi [\varepsilon^{-1}(x - x_0)], \quad (4.2)$$

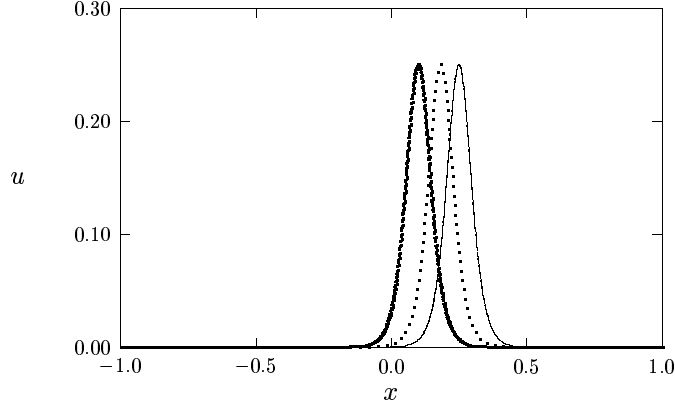


Figure 3: Plot of u at different times from the numerical solution to (1.3) with $D = 1.0$, $\tau = 0$, and $\varepsilon = 0.03$. The solid curve is at $t = 0$, the dashed curve is at $t = 2190$, and the heavy solid curve is at $t = 6108$

where $\Phi(y) \rightarrow 0$ exponentially as $|y| \rightarrow \infty$. Since a_c and ϕ are localized near $x = x_0$, the problem (4.1b) for η reduces, for $\varepsilon \rightarrow 0$, to

$$D\eta_{xx} - (1 + \tau\lambda)\eta = 0, \quad -1 < x < 1; \quad \eta_x(\pm 1) = 0, \quad (4.3a)$$

$$[\eta]_0 = 0, \quad [D\eta_x]_0 = -\omega + sb_m H^\zeta \eta(x_0), \quad (4.3b)$$

where

$$\omega \equiv mH^{\gamma(m-1)-s} \int_{-\infty}^{\infty} w^{m-1} \Phi dy. \quad (4.3c)$$

In (4.3b), we have defined $[v]_0 \equiv v(x_{0+}) - v(x_{0-})$. Similarly, for $\varepsilon \ll 1$, the problem (4.1a) in terms of Φ becomes

$$\Phi'' - \Phi + pw^{p-1}\Phi - qH^{\gamma-1}w^p\eta(x_0) = \lambda\Phi, \quad -\infty < y < \infty. \quad (4.4)$$

By solving (4.3) explicitly, we can calculate $\eta(x_0)$ as

$$\eta(x_0) = \frac{\omega}{D\theta_\lambda\beta(\theta_\lambda; x_0) + sH^\zeta b_m}, \quad (4.5)$$

where $\theta_\lambda \equiv \sqrt{(1 + \tau\lambda)/D}$, and the function $\beta(\xi; x_0)$ is defined by

$$\beta(\xi; x_0) \equiv \tanh[\xi(1 + x_0)] + \tanh[\xi(1 - x_0)]. \quad (4.6)$$

Next, we substitute $b_m H^\zeta = [G_m(x_0; x_0)]^{-1}$, obtained from (3.1f), into (4.5). By calculating $G_m(x_0; x_0)$ explicitly from (3.1e), we find $[G_m(x_0; x_0)]^{-1} = \sqrt{D}\beta(\theta_0; x_0)$, where $\theta_0 = D^{-1/2}$. Substituting the resulting expression for $\eta(x_0)$ into (4.4), we obtain the following nonlocal eigenvalue problem:

Proposition 4.1: *Assume that $0 < \varepsilon \ll 1$, $\tau \geq 0$, and $x_0 \in (-1, 1)$. Then, the stability of the quasi-equilibrium profile (3.1a) and (3.1b) for the GM model (1.1) is determined by the spectrum of the nonlocal eigenvalue problem*

$$L_0\Phi - \chi_m w^p \left(\frac{\int_{-\infty}^{\infty} w^{m-1} \Phi dy}{\int_{-\infty}^{\infty} w^m dy} \right) = \lambda \Phi, \quad -\infty < y < \infty, \quad (4.7a)$$

$$\Phi \rightarrow 0, \quad \text{as } |y| \rightarrow \infty. \quad (4.7b)$$

In (4.7), the local operator L_0 , and the multiplier χ_m are defined by,

$$L_0\Phi \equiv \Phi'' - \Phi + pw^{p-1}\Phi, \quad (4.7c)$$

and

$$\chi_m = \chi_m(z; x_0) \equiv qm \left[s + \sqrt{1+z} \left(\frac{\beta(\theta_\lambda; x_0)}{\beta(\theta_0; x_0)} \right) \right]^{-1}. \quad (4.7d)$$

Here the function $\beta(\xi; x_0)$ is defined in (4.6), and

$$z \equiv \tau\lambda, \quad \theta_\lambda \equiv \theta_0 \sqrt{1+z}, \quad \theta_0 \equiv D^{-1/2}. \quad (4.7e)$$

We now formulate a nonlocal eigenvalue problem that determines the stability of a one-spike quasi-equilibrium profile for the Schnakenburg model (1.3). Since the details of the analysis are similar to that given above for the GM model, we simply outline the key steps in the derivation. For a fixed $x_0 \in (-1, 1)$, the quasi-equilibrium profile u_c, v_c for (1.3) is defined in (3.3). Substituting $u = u_c + e^{\lambda t}\phi$ and $v = v_c + e^{\lambda t}\eta$, with $\phi \ll 1$ and $\eta \ll 1$, into (1.3), we obtain the eigenvalue problem

$$\varepsilon^2 \phi_{xx} - \phi + 2u_c v_c \phi + u_c^2 \eta = \lambda \phi, \quad -1 < x < 1, \quad (4.8a)$$

$$D\eta_{xx} - \tau\lambda\eta = 2\varepsilon^{-1}u_c v_c \phi + \varepsilon^{-1}u_c^2 \eta, \quad -1 < x < 1, \quad (4.8b)$$

$$\phi_x(\pm 1) = \eta_x(\pm 1) = 0. \quad (4.8c)$$

We look for a localized eigenfunction of (4.8) in the form (4.2). In place of (4.3), we now obtain

$$D\eta_{xx} - \tau\lambda\eta = 0, \quad -1 < x < 1; \quad \eta_x(\pm 1) = 0, \quad (4.9a)$$

$$[\eta]_0 = 0, \quad [D\eta_x]_0 = \frac{\eta(x_0)}{V} + 2 \int_{-\infty}^{\infty} w\Phi dy. \quad (4.9b)$$

Here V is defined in (3.12). From (4.8a), the eigenvalue problem for Φ becomes

$$\Phi'' - \Phi + 2w\Phi + V^{-2}w^2\eta(x_0) = \lambda\Phi, \quad -\infty < y < \infty. \quad (4.10)$$

By solving (4.9) explicitly, we can calculate $\eta(x_0)$. Substituting this formula for $\eta(x_0)$ into (4.10), we obtain the following nonlocal eigenvalue problem analogous to (4.7):

Proposition 4.2: *Assume that $0 < \varepsilon \ll 1$, $\tau \geq 0$, and $x_0 \in (-1, 1)$. Then, the stability of the quasi-equilibrium profile (3.3a) and (3.3b) for the Schnakenburg model (1.3) is determined by the spectrum of the nonlocal eigenvalue problem*

$$L_0\Phi - \chi_s w^2 \left(\frac{\int_{-\infty}^{\infty} w\Phi dy}{\int_{-\infty}^{\infty} w^2 dy} \right) = \lambda\Phi, \quad -\infty < y < \infty, \quad (4.11a)$$

$$\Phi \rightarrow 0, \quad \text{as } |y| \rightarrow \infty. \quad (4.11b)$$

Here L_0 and w satisfy (4.7c) and (3.1d), respectively, with $p = 2$. The multiplier χ_s is defined by

$$\chi_s = \chi_s(z; x_0) \equiv 2 \left[1 + 6\sqrt{Dz}\beta(\mu_\lambda; x_0) \right]^{-1}, \quad z \equiv \tau\lambda, \quad \mu_\lambda \equiv \sqrt{z/D}. \quad (4.11c)$$

In (4.11c), the function $\beta(\xi; x_0)$ is defined in (4.6).

4.2 Numerical Computations of the Spectrum: Small-Scale Oscillations

In this section we determine, numerically, conditions for which a complex conjugate pair of eigenvalues for (4.7) and (4.11) crosses into the unstable right half-plane $\text{Re}(\lambda) > 0$ as τ is increased. For illustration purposes, in the remainder of §4 our computations for the GM model (1.1) are done only for the exponent set $(p, q, m, s) = (2, 1, 2, 0)$. A much more detailed analysis of the spectrum of the GM nonlocal eigenvalue problem (4.7) is given in [31].

We first reformulate (4.11) and (4.7). Let $\psi(y)$ be the solution to

$$L_0\psi = \lambda\psi + w^2; \quad \psi \rightarrow 0 \quad \text{as } |y| \rightarrow \infty. \quad (4.12)$$

Here $w(y) = \frac{3}{2}\text{sech}^2(y/2)$. Then, the eigenfunctions of (4.7) and (4.11) can be written as

$$\phi = J\chi\psi, \quad J \equiv \frac{\int_{-\infty}^{\infty} w\phi dy}{\int_{-\infty}^{\infty} w^2 dy}, \quad (4.13)$$

where χ is either χ_m or χ_s . We are only interested in eigenfunctions for which $\int_{-\infty}^{\infty} w\phi dy \neq 0$. If $\int_{-\infty}^{\infty} w\phi dy = 0$, then they must be the translation mode of the local operator L_0 . This mode is w' , and it corresponds only to the zero eigenvalue. Thus, from multiplying (4.13) by w and integrating, we obtain that the eigenvalues of the nonlocal eigenvalue problems are the roots of $g(\lambda) = 0$, where

$$g(\lambda) \equiv \frac{1}{\chi} - \frac{\int_{-\infty}^{\infty} w\psi dy}{\int_{-\infty}^{\infty} w^2 dy}. \quad (4.14)$$

When $D = \infty$ and $\tau = 0$, it was proved in [32] that $\text{Re}(\lambda) < 0$, except for the translation mode $\phi = w'$ where $\lambda = 0$.

We now look for a pure imaginary eigenvalue of the form $\lambda = i\lambda_I$. Without loss of generality we may assume that $\lambda_I > 0$. Along the imaginary axis, we separate (4.14) and (4.12) into real and imaginary parts by writing

$$g = g_R + ig_I, \quad \lambda = i\lambda_I, \quad \psi = \psi_R + i\psi_I. \quad (4.15)$$

From (4.14) and (4.12) we get

$$g_R \equiv \text{Re} \left(\frac{1}{\chi} \right) - \frac{\int_{-\infty}^{\infty} w\psi_R dy}{\int_{-\infty}^{\infty} w^2 dy}, \quad g_I \equiv \text{Im} \left(\frac{1}{\chi} \right) - \frac{\int_{-\infty}^{\infty} w\psi_I dy}{\int_{-\infty}^{\infty} w^2 dy}, \quad (4.16)$$

where

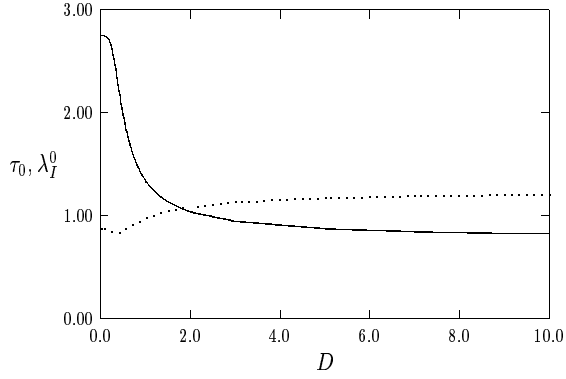
$$L_0\psi_R = -\lambda_I\psi_I + w^p; \quad L_0\psi_I = \lambda_I\psi_R, \quad (4.17)$$

with $\psi_R \rightarrow 0$ and $\psi_I \rightarrow 0$ as $|y| \rightarrow \infty$.

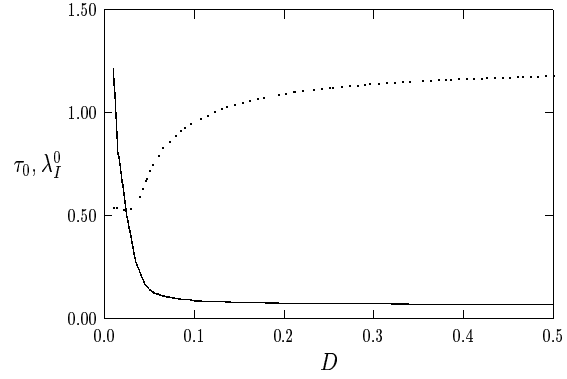
The coupled system $g_R = 0$ and $g_I = 0$ gives two equations for λ_I and τ for given values of D and x_0 . These critical values of τ and λ_I are labeled by τ_0 by λ_I^0 . Our numerical computations below determine the *minimum* value of τ for which a complex conjugate pair of eigenvalues crosses into the right half-plane. To compute τ_0 and λ_I^0 we solve the system (4.17) for ψ_R and ψ_I numerically using COLSYS at each fixed λ_I . We then use Newton's method to locate the roots to $g_R = 0$ and $g_I = 0$, and we use Euler continuation to calculate the dependence of τ_0 on x_0 and on D . We have verified numerically that these eigenvalues cross into the right half-plane as τ is increased past τ_0 .

In Fig 4(a) we plot τ_0 and λ_I^0 versus D for a spike of the GM model (1.1) with $(p, q, m, s) = (2, 1, 2, 0)$ that is located at the origin $x_0 = 0$. When $x_0 = 0$, τ_0 is a monotonically decreasing function of D . It ranges from the value $\tau_0 \approx 2.749$ when $D \ll 1$, to $\tau_0 \approx 0.771$ when $D \gg 1$. Thus, to obtain an oscillatory instability as D is decreased, we must increase the value of τ . From Fig. 4(a) we see that the frequency λ_I^0 of small oscillations has a weak dependence on D and is quite close to the value unity for the full range of D . Similarly, in Fig 4(b) we plot τ_0 and λ_I^0 versus D for a spike of the Schnakenburg model (1.3) that is located at the origin $x_0 = 0$. Once again τ_0 is a decreasing function of D , and $\tau_0 \rightarrow 0.065$ as $D \rightarrow \infty$. However, in contrast to the GM model, τ_0 is unbounded as $D \rightarrow 0$. This difference between the models results from the fact that χ_m in (4.7d) is such that χ_m^{-1} is independent of D for $D \ll 1$, whereas for the Schnakenburg model with $x_0 = 0$ we have from (4.11c) that $\chi_s^{-1} \rightarrow \frac{1}{2} + 6\sqrt{D\tau\lambda}$ for $D \ll 1$. Also note that τ_0 has already decreased to its limiting value $\tau_0 \approx 0.065$ when $D > 0.2$. Thus, unless D is very small, oscillatory instabilities in the Schnakenburg model will typically occur for smaller values of τ than for the GM model with $(p, q, m, s) = (2, 1, 2, 0)$.

We now give a numerical confirmation of our results predicting the onset of an oscillatory instability. To do so, we solve the GM model (1.1) and the Schnakenburg model (1.3) numerically using the moving-mesh method of §2. Results essentially identical to those displayed are obtained

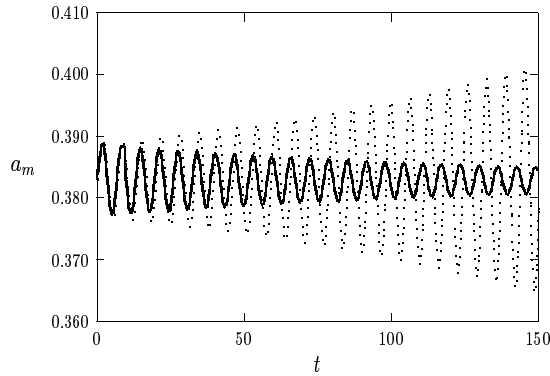


(a) GM model: $(p, q, m, s) = (2, 1, 2, 0)$, $x_0 = 0$

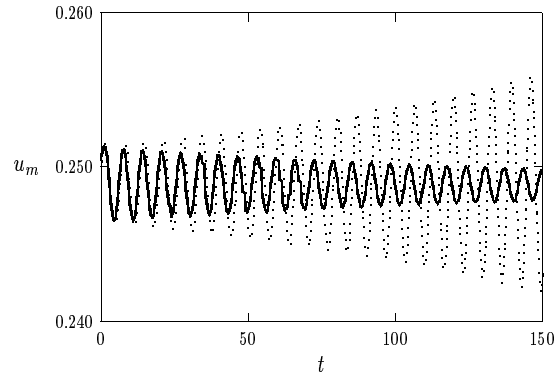


(b) Schnakenburg model: $x_0 = 0$

Figure 4: Plots of τ_0 (solid curve) and λ_I^0 (dashed curve) for the GM model (leftmost figure) and the Schnakenburg model (rightmost figure).



(a) GM model: $x_0 = 0$, $D = 1.0$, $\varepsilon = 0.01$.



(b) Schnakenburg model: $x_0 = 0$, $D = 0.1$, $\varepsilon = 0.01$

Figure 5: Plots of a_m versus t for the GM model in the leftmost figure with $\tau = 1.3$ (heavy solid curve) and $\tau = 1.35$ (dashed curve). In the rightmost figure we plot u_m versus t for the Schnakenburg model with $\tau = 0.085$ (heavy solid curve) and $\tau = 0.088$ (dashed curve).

using the NAG library routine D03PCF [18]. The initial condition for the GM model (1.1) is taken to be a small, but localized, perturbation off of the equilibrium solution a_c and h_c given in (3.1) with $x_0 = 0$. More precisely, we took

$$a(x, 0) = a_c \left[1 + 0.02 \cos \left(\frac{\pi x}{\varepsilon} \right) e^{-x^2/(2\varepsilon)} \right], \quad h(x, 0) = h_c. \quad (4.18)$$

A similar small perturbation off of the equilibrium solution u_c and v_c , given in (3.3), is used in the numerical simulation of the Schnakenburg model (1.3).

To illustrate small-scale oscillatory behavior for the GM model, in Fig. 5(a) we plot $a_m \equiv a(0, t)$, referred to as the amplitude of the spike, as a function of t for two values of τ when $D = 1$ and $\varepsilon = 0.01$. Numerically, from the data used to generate Fig. 4(a), we get that $\tau_0 = 1.343$. Notice from Fig. 5(a) that, when $\tau = 1.3$, the small oscillations generated by the perturbation are damped out, whereas when $\tau = 1.35$ the oscillations begin to grow as t increases. Similarly, for the Schnakenburg model, in Fig. 5(b) we plot $u_m \equiv u(0, t)$ as a function of t for two values of τ when $D = 0.1$ and $\varepsilon = 0.01$. The value predicted from the nonlocal eigenvalue problem is $\tau_0 = 0.0873$. From Fig. 5(b) we observe that small oscillations are damped out when $\tau = 0.085$ and they begin to grow when $\tau = 0.088$. We have performed similar tests for other parameter values to obtain confirming evidence of the oscillatory instability that occurs when τ is increased beyond the critical value τ_0 . The resulting Hopf bifurcation is apparently subcritical as numerical evidence suggests that the emerging small-scale periodic oscillations are unstable.

4.3 Large-Scale Oscillations: Spike at the Origin

We now illustrate some large-scale oscillatory motions that occur for a spike centered at the origin $x_0 = 0$ when τ is well beyond the bifurcation value τ_0 . Starting from the initial condition (4.18), in Fig. 6(a) and Fig. 6(b) we plot the numerically computed spike amplitude $a_m \equiv a(0, t)$ versus t for $\tau = 1.38$ and $\tau = 1.5$. The parameters for the GM model are $D = 1$, $\varepsilon = 0.01$, and $(p, q, m, s) = (2, 1, 2, 0)$. The critical value τ_0 for these parameters is $\tau_0 = 1.343$. Notice that when $\tau = 1.5$, the amplitude of the spike exhibits a few large oscillations for some range of t , but then eventually collapses to zero. Similar spike collapse behavior occurs for larger values of τ . However, when $\tau = 1.38$ we observe a very intricate large-scale motion in the spike amplitude. This type of motion, which persists for long time intervals, has not been observed previously for (1.1). Although the spike remains at the origin, a numerical solution requires small time-steps and an accurate time integration scheme to capture the oscillations. The intricate oscillatory motion is not due to numerical errors as it persists under grid refinement and was also verified using the NAG library routine D03PCF [18]. A related oscillatory behavior was found in [30] for the N -dimensional shadow GM problem obtained by taking the limit $D \rightarrow \infty$ in the multi-dimensional extension of (1.1). The qualitative mechanism responsible for this behavior in the shadow system is given in [30]. The analysis of the oscillation shown in Fig. 6 is an open problem.

Similar oscillatory behavior occur for the Schnakenburg model when τ is increased past the critical value τ_0 . In Fig. 7(a) and Fig. 7(b) we plot the numerically computed spike amplitude

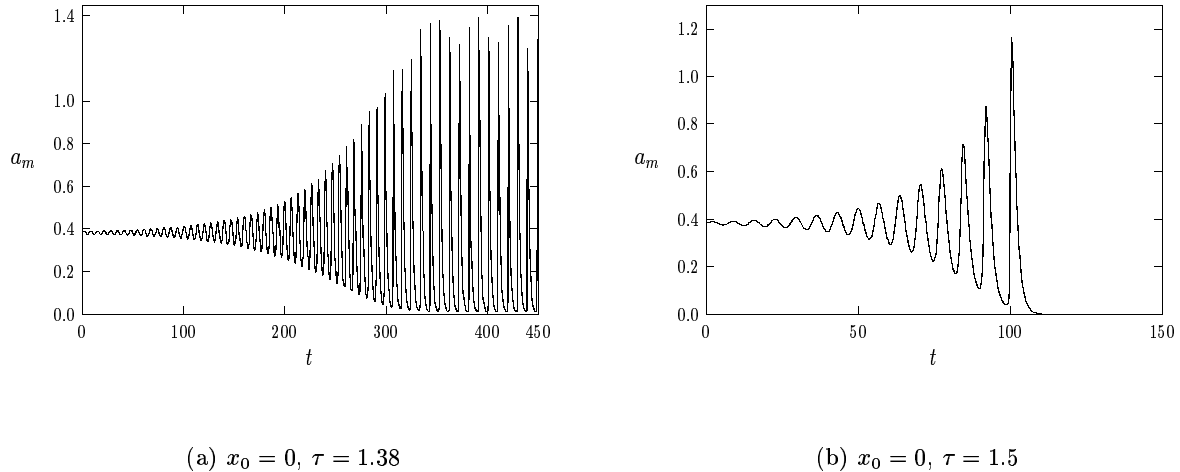


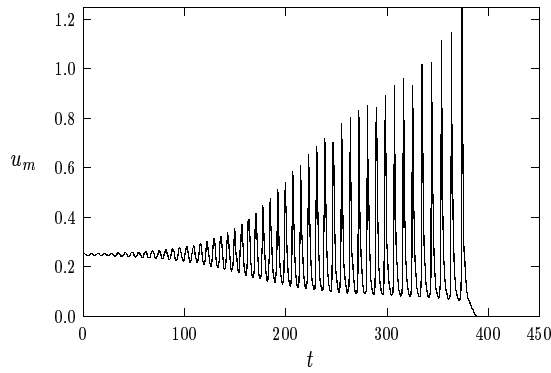
Figure 6: Plots of a_m versus t for the GM model at two values of τ when $D = 1.0$ and $\varepsilon = .01$.

$u_m \equiv u(0, t)$ versus t for $\tau = 0.092$ and $\tau = 0.10$, when $D = 1$ and $\varepsilon = 0.01$. The critical value τ_0 is $\tau_0 = 0.0873$. When τ is sufficiently beyond the value τ_0 , the spike amplitude tends to zero as t increases, such as in Fig. 7(b) for $\tau = 0.10$. However, as seen in Fig. 7(a), for intermediate values of τ such as $\tau = 0.092$, the spike amplitude exhibits a large-scale oscillatory motion persisting for long time intervals, before it eventually collapses.

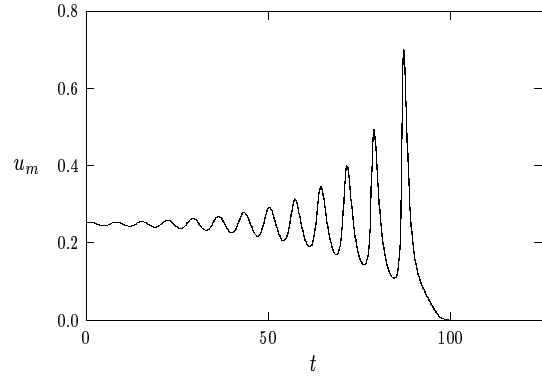
4.4 Large-Scale Oscillations: Slowly Drifting Spikes

Next we consider instabilities that occur for quasi-equilibrium solutions where the spike is initially located at some $x_0 \in (-1, 1)$. By symmetry τ_0 is an even function of x_0 and so we need only consider $x_0 \in (0, 1)$. From the numerical procedure described in §4.2, we can calculate the dependence of τ_0 on $x_0 \in (0, 1)$ for different values of D . In the remainder of this section we write $\tau_0 = \tau_0(x_0)$. For different values of D , the results are shown in Fig. 8(a) for the GM model with $(p, q, m, s) = (2, 1, 2, 0)$ and in Fig. 8(b) for the Schnakenburg model. The behavior of τ_0 as a function of x_0 depends on the value of D and is complicated. For $D \gg 1$, τ_0 is constant with respect to x_0 . For larger values of D , we find that τ_0 is an increasing function of x_0 (see the curves in Fig. 8(a) and Fig. 8(b) for $D = 1.0$ and $D = 0.1$, respectively). For smaller values of D , the dependence of τ_0 on x_0 is not monotone. The results shown in these figures for $x_0 \rightarrow 1$ give the critical value τ_0 for a boundary spike on an interval of length 2. This value is the same as the threshold for a spike centered at the origin in a domain of length 4.

The dependence $\tau_0 = \tau_0(x_0)$ suggests that we look for sudden oscillatory instabilities for slowly

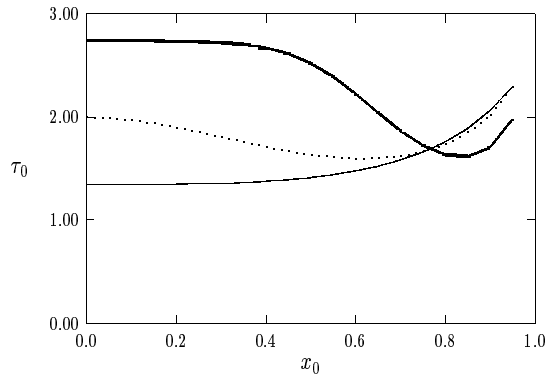


(a) $x_0 = 0$, $D = 0.1$, $\tau = 0.092$

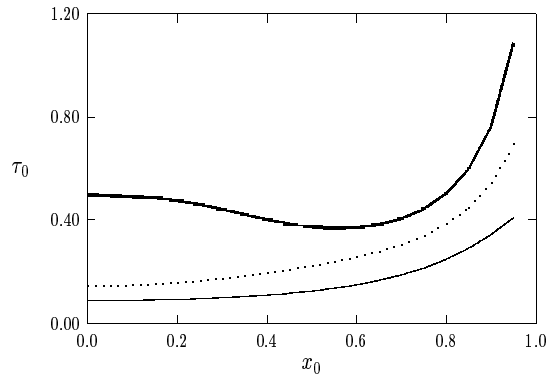


(b) $x_0 = 0$, $D = 0.1$, $\tau = 0.10$

Figure 7: Plots of u_m versus t for the Schnakenburg model with $D = 0.10$ and $\varepsilon = 0.01$ at two different values of τ .



(a) GM model: $(p, q, m, s) = (2, 1, 2, 0)$



(b) Schnakenburg model

Figure 8: Plots of τ_0 versus x_0 for the GM model and Schnakenburg model. In the leftmost figure, $D = 1.0$ (solid curve), $D = 0.5$ (dashed curve), and $D = 0.1$ (heavy solid curve). In the rightmost figure, $D = 0.1$ (solid curve), $D = 0.05$ (dashed curve), and $D = 0.025$ (heavy solid curve).

drifting spikes. In particular, for certain choices of τ and the initial spike location $x_0(0)$, this dependence of τ_0 on x_0 suggests that at some point during the slow evolution of a spike, a sudden and very intricate oscillatory motion in its height, occurring on an $O(1)$ time-scale, can develop. The four experiments below show precisely this feature. The numerical results displayed below were computed using the NAG library software D03PCF [18] with 2000 spatial meshpoints and stringent tolerances on the local accuracy of each time-step. The phenomena persists under spatial grid refinement and the usual numerical tests. The moving mesh-method performed adequately in computing these intricate behaviors.

In each of the experiments below, the initial condition for the GM model (1.1) was a perturbation of the form (4.18) of the quasi-equilibrium solution centered at x_0 , with a similar form for the Schnakenburg model. The location $x = x_0(t)$ of the maximum of either a for (1.1) or u for (1.3) is plotted together with the maximum values $a_m = a(x_0, t)$ and $u_m = u(x_0, t)$.

Experiment 1 (GM Model): Persistent Oscillation: We take $D = 1.0$, $\varepsilon = 0.03$, $\tau = 1.35$, $x_0(0) = 0.6$, and $(p, q, m, s) = (2, 1, 2, 0)$. For $D = 1.0$, $\tau_0(x_0)$ is a monotonically increasing function of x_0 for $x_0 > 0$ (see Fig. 8(a)). Key critical values of $\tau_0(x_0)$ are $\tau_0(0.6) = 1.477$, $\tau_0(0) = 1.343$ and $\tau_0(0.35) = 1.36$. Since $\tau < \tau_0(0.6)$, the spike is initially stable. It then slowly drifts towards the origin. However, since $\tau(0) < \tau$ it experiences a sudden instability before it reaches the origin. A plot of the spike amplitude $a_m(t)$ and spike location $x_0(t)$ are shown in Fig. 9(a) and Fig. 9(b), respectively. The oscillation for a_m , which is shown on a shorter time interval than for x_0 only for graphical purposes, persists for a very long-time interval. Recall that with the same parameter values, but with $\tau = 0$, the corresponding motion was computed previously in Experiment 1 of §3.

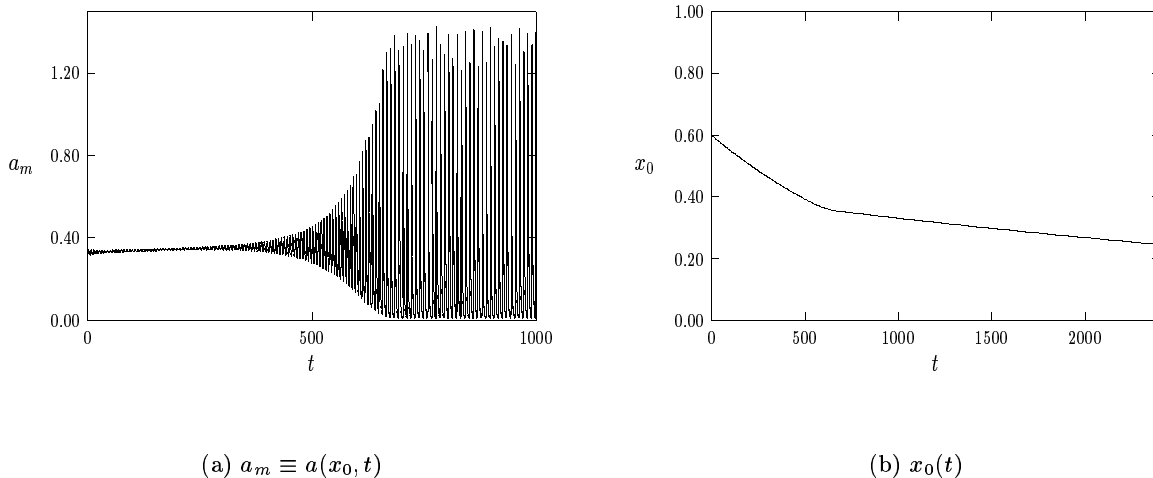


Figure 9: Plots of a_m and x_0 versus t for Experiment 1 of §4.3.

Experiment 2 (GM Model): Oscillation Followed by Collapse: We take $D = 1.0$, $\varepsilon = 0.03$, $\tau = 1.42$, $x_0(0) = 0.6$, and $(p, q, m, s) = (2, 1, 2, 0)$. The only difference between this and the previous experiment is that we have raised the value of τ . In this case, the spike begins to drift slowly towards the origin, but then collapses to zero. The numerical results are shown In Fig. 10(a) and Fig. 10(b), respectively. This example is qualitatively similar to the example of §4.2 where, for a spike at the origin, the value of τ well exceeds the Hopf bifurcation value τ_0 .

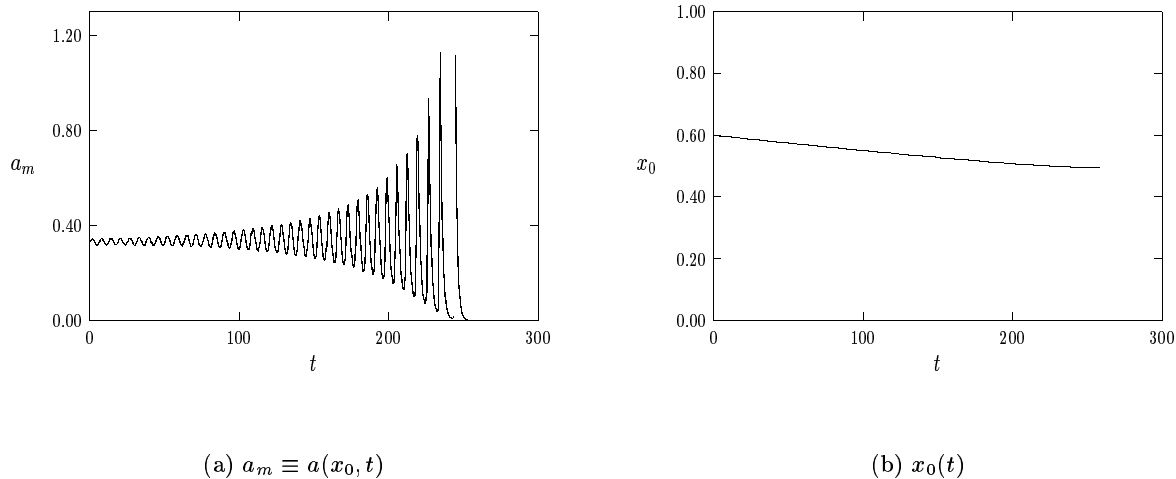


Figure 10: Plots of a_m and x_0 versus t for Experiment 2 of §4.3.

Experiment 3 (Schnakenburg): A Delayed Oscillatory Collapse: We take $D = 0.05$, $\varepsilon = 0.015$, $\tau = 0.2$ and $x_0(0) = 0.5$. For this value of D , we obtain from Fig. 8(b) that $\tau_0(x_0)$ is monotonically increasing. Key critical values of $\tau_0(x_0)$ are $\tau_0(0.5) = 0.22$, $\tau_0(0.4) = 0.194$, and $\tau_0(0.35) = 0.182$. As shown in Fig. 11(a) and Fig. 11(b), the spike begins to drift towards the origin. It then experiences a sudden instability, and then ultimately collapses. Notice, however, that there is a delayed bifurcation effect in that the spike is able to penetrate some distance into the unstable region before the instability is triggered. This phenomena occurs since the initial perturbation in the spike amplitude has essentially completely died out before the spike enters the zone of instability. Similar types of delayed bifurcation phenomena are well-known in ODE models.

Experiment 4 (Schnakenburg): Persistent Oscillation: We take $D = 0.025$, $\varepsilon = 0.01$, $\tau = 0.459$ and $x_0(0) = 0.25$. For this value of D , we have from Fig. 8(b) that $\tau_0(x_0)$ is monotonically decreasing on $0 \leq x_0 \leq 0.25$. Key critical values are $\tau_0(0) = 0.497$ and $\tau_0(0.25) = 0.459$. Thus, for this example, the initial spike location is chosen so that $\tau = \tau_0$. Hence a small-scale oscillation should emerge initially. In Fig. 12(a) and Fig. 12(b) we plot u_m and x_0 versus t . The spike moves towards the origin into a region of stability where $\tau < \tau_0(x_0)$. Notice that the small-scale oscillation

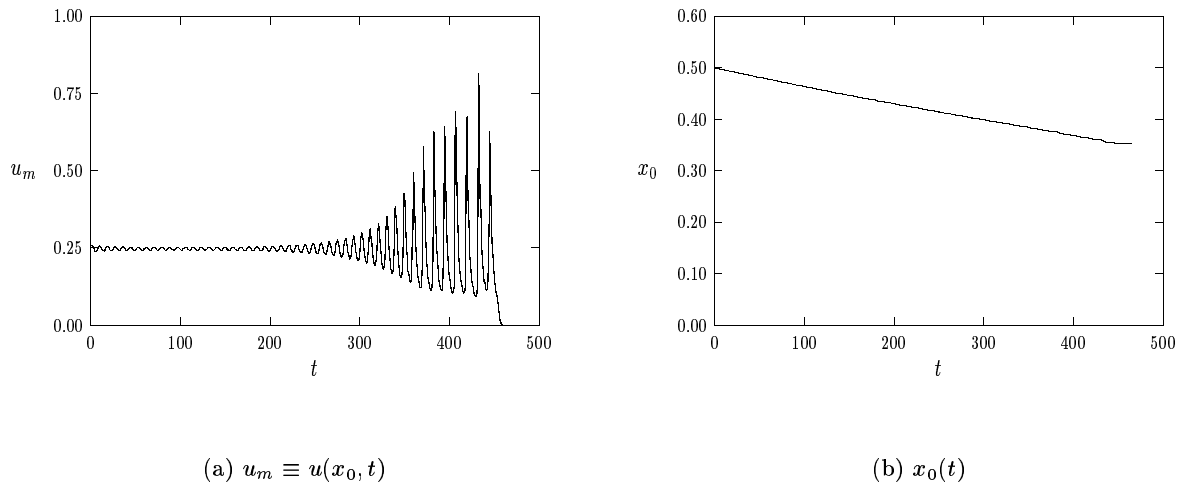


Figure 11: Plots of u_m and x_0 versus t for Experiment 3 of §4.3.

persists for a very long time interval, but is slowly damped out as the spike approaches the origin. The approach of the spike to the origin is monotonic. Again, for graphical purposes only, we have plotted u_m on a shorter time interval than x_0 .

Further numerical experiments have revealed three interesting qualitative features of this type of oscillatory instability: (1) There is no significant qualitative difference in the behavior between the GM model and the Schnakenburg model with respect to these oscillations. (2) The spike always appears to drift slowly towards the origin, rather than towards the boundary of the domain. This occurs even if the function $\tau_0(x_0)$ has a minimum at some point x_0^* in $(0, 1)$, such as shown in Fig. 8(a) for the GM model where for $D = 0.50$ we have $x_0^* \approx 0.67$. If we choose $x_0(0) > x_0^*$ and $\tau > \tau_0(x_0^*)$, the spike will attempt to move to the origin through the unstable zone rather than in the direction of the boundary where it would not experience a sudden instability. (3) The motion of the spike is monotonic towards the origin, but its speed slows when there is an oscillatory instability in the height of the spike (see the kink in the graph of Fig. 9(b)). The derivation of an explicit equation of motion of the spike for (1.1) and (1.3) when $\tau > 0$, in a form similar to that given in propositions 3.1 and 3.2, is an open problem.

The type of intricate oscillatory instability observed above, which is initially triggered through a subcritical Hopf bifurcation, has not been observed previously. In [23] it was shown that the Gray-Scott model can exhibit various types of chaotic pulse dynamics in certain parameter regimes when the two diffusion coefficients in the model are of the same asymptotic order. The irregular behavior observed above is significantly different in that it occurs for an $O(1)$ inhibitor diffusivity and an $O(\varepsilon^2)$ activator diffusivity.

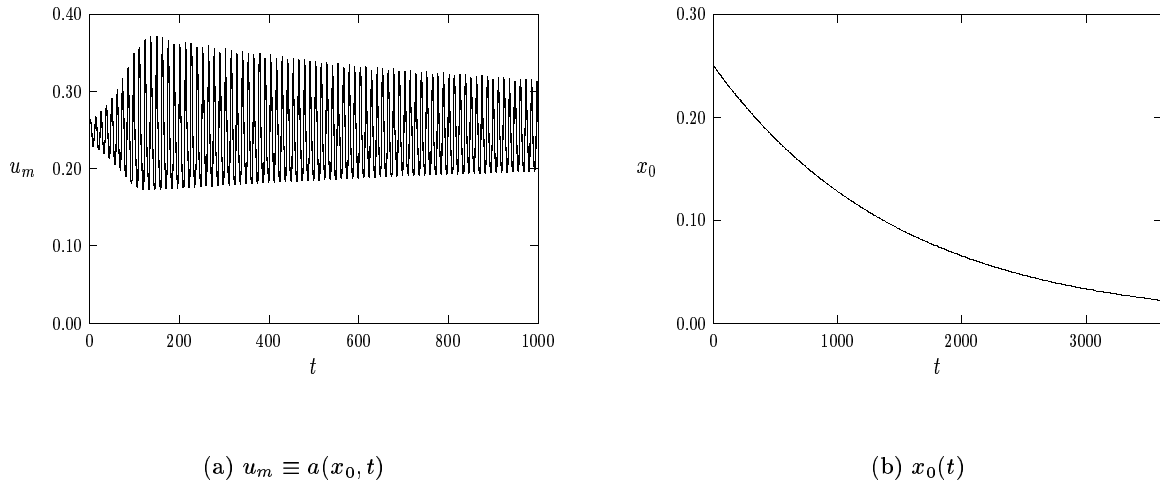


Figure 12: Plots of u_m and x_0 versus t for Experiment 4 of §4.3.

5 Pulse-Splitting Dynamics with Small Inhibitor Diffusion

When D is sufficiently small, with $D = O(\varepsilon^2)$, pulse-splitting can occur in the GM model (1.1) (cf. [8], [21]). For a certain range of the parameters, an initial one-spike profile centered at the midpoint of the domain can split into two spikes that travel towards the ends of the interval. Each of these spikes can then in turn split again. The splitting process can continue until a sequence of oscillations fills up the domain. Related pulse-splitting instabilities for the Gray-Scott model were computed numerically in [25], and then analyzed in detail in [5], [6], [7], and [22]. In [22], a detailed mechanism for pulse-splitting was put forth, with one key feature being that pulse-splitting is linked to the disappearance of branches of homoclinic orbits.

For the GM model, pulse-splitting was observed in [8] in their analysis of bifurcations of homoclinic stripe patterns in thin two-dimensional domains. It was also predicted by [21]. Similar to the mechanism in the Gray-Scott model, pulse-splitting in the GM model seems to be related to the disappearance of a homoclinic orbit, which approximates the solution in the core of the spike, as D is decreased below some critical value. It is beyond our scope here to give a full account of pulse-splitting behavior for (1.1). Instead we give a numerical procedure to identify the critical value of D below which pulse-splitting should occur. We then give an example to validate our prediction, and show that the moving-mesh method of §2 is able to calculate the solution.

When $D = O(\varepsilon^2)$, the analysis leading to the quasi-equilibrium profiles a_c and h_c in (3.1) is invalid. However, by letting $D = O(\varepsilon^2)$ in (3.1b) we can determine the appropriate scalings for studying pulse-splitting behavior. Setting $D = O(\varepsilon^2)$ in (3.1e), we calculate from (3.1f) and (3.1b)

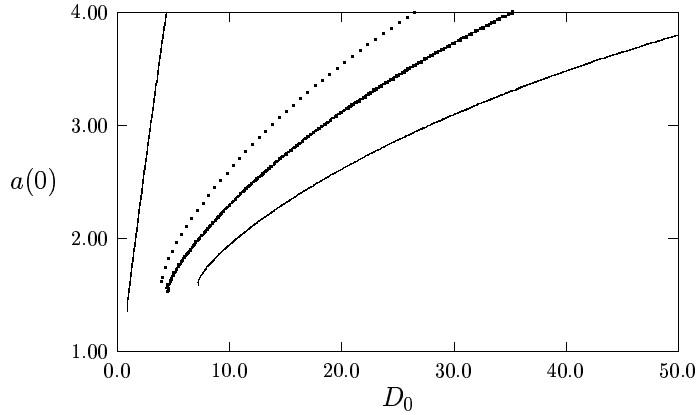


Figure 13: Plots of $a(0)$ versus D_0 for the homoclinic orbit of (5.2) for different exponent sets. The top curve is for $(4, 2, 2, 0)$, the dashed curve is for $(3, 2, 2, 0)$, the heavy solid curve is for $(3, 2, 3, 1)$, and the solid curve is for $(2, 1, 2, 0)$. In each case, numerical evidence indicates that the solution branch cannot be continued below the minimum value of D_0 shown on each curve.

that $h = O(\varepsilon^{1/\zeta})$ as $\varepsilon \rightarrow 0$ near the core of the spike. Here ζ is given in (1.2). This suggests the following rescaling in the spike core:

$$h = \varepsilon^{1/\zeta} \tilde{h}, \quad a = \varepsilon^{q/(p-1)\zeta} \tilde{a}, \quad D = \varepsilon^2 D_0, \quad y = \varepsilon^{-1}(x - x_0). \quad (5.1)$$

Substituting (5.1) into the steady-state form of (1.1), and dropping the tilde notation, we obtain

$$a_{yy} - a + a^p/h^q = 0, \quad 0 < y < \infty, \quad (5.2a)$$

$$D_0 h_{yy} - h + a^m/h^s = 0, \quad 0 < y < \infty, \quad (5.2b)$$

with the symmetry condition $h'(0) = a'(0) = 0$. We look for solutions to this problem for which $a \rightarrow 0$ as $y \rightarrow \infty$ and h is bounded as $y \rightarrow \infty$. To do so, we compute solutions to (5.2) numerically on a large but finite domain $0 < y < y_r$. We start from a large value of D_0 , where we have an initial point on the solution branch given by the shadow solution $a = H^\gamma w(y)$ with $\gamma = q/(p-1)$ and $H^\zeta = y_r [\int_0^{y_r} w^m dy]^{-1}$. Here w satisfies (3.1d). We then compute the solution branch to (5.2) using the boundary value solver COLSYS [1] as D_0 is decreased. In each case, we found that the numerical procedure fails to converge at some critical value $D_0 = D_c$, where the homoclinic solution for a and h disappears. In Fig. 13 we plot the numerically computed value of $a(0)$ versus D_0 . For different exponent sets (p, q, m, s) , the critical value D_c is found to be

$$D_c = 7.171, \quad (2, 1, 2, 0); \quad D_c = 3.905, \quad (3, 2, 2, 0), \quad (5.3a)$$

$$D_c = 4.410, \quad (3, 2, 3, 1); \quad D_c = 0.886, \quad (4, 2, 2, 0). \quad (5.3b)$$

The results below were verified to be independent of y_r , when $y_r > 15$. An estimate for D_c for the exponent set $(2, 1, 2, 0)$ was obtained by another approach in [8]. They found $D_c = 1/1.4 \approx 7.143$. In terms of the original variables, the critical value of D is $D = \varepsilon^2 D_c$. The results for D_c for the other exponent sets have not been reported previously.

Qualitatively, the reason why the homoclinic orbit for a disappears as D_0 is decreased below some critical value, is because when D_0 is small, h decreases very fast, and h may decrease faster than a for $y \gg 1$. Thus, the term a^p/h^q in (5.2a) may grow as $y \rightarrow \infty$. When this condition occurs, it certainly precludes the existence of a homoclinic orbit. A simple-minded approach to get a bound on D_c , is to analyze the tail behavior for a and h as $y \rightarrow \infty$. In this tail region we assume that $a \ll 1$ and $h \ll 1$. We then introduce a small parameter δ by $a = \delta^\gamma \hat{a}$ and $h = \delta \hat{h}$. The equation (5.2b) for h transforms to $D_0 \hat{h}_{yy} - \hat{h} + \delta^\zeta \tilde{a}^m / \hat{h}^s = 0$. Since $\zeta > 0$, we get that $\hat{h} \sim c_h e^{-y/\sqrt{D_0}}$ for some $c_h > 0$ when $\delta \ll 1$. The equation for \hat{a} becomes

$$\hat{a}_{yy} - \hat{a} + c_h^{-q} \hat{a}^p e^{qy/\sqrt{D_0}} = 0. \quad (5.4)$$

For $y \gg 1$, we let $\hat{a} = c_a e^{-\sigma y}$. Substituting this into (5.4), and ensuring that we have exponential decay as $y \rightarrow \infty$, we require that

$$\sigma^2 - 1 > 0, \quad \sigma(1-p) + \frac{q}{\sqrt{D_0}} > 0. \quad (5.5)$$

The minimum conditions for decay is when we have equality in (5.5). Setting $\sigma = 1$, we get the prediction that there is no homoclinic orbit if $D_0 < [q/(p-1)]^2$. This simple-minded approach gives a bound on the critical value D_c but, as seen from (5.3), this bound is not that close to the actual computed value. However, this calculation in the tail region does give a qualitative explanation why the homoclinic orbit ceases to exist as D_0 is decreased. Furthermore, it suggests that D_c should decrease as p increases. This is seen from the results in (5.3).

Experiment: As an example, we choose $\varepsilon = 0.03$ and the exponent set $(p, q, m, s) = (2, 1, 2, 0)$. For these parameter values, we predict from (5.3) that pulse-splitting will occur when $D < 0.00645$. To test this prediction, we take $D = 0.006$, and $\tau = 0.05$. The initial condition, with a spike at the origin, is taken to be a small perturbation from the quasi-equilibrium solution a_c and h_c , given in proposition 3.1, evaluated at $x_0 = 0$, $D = 0.006$, $\varepsilon = 0.03$, and with $(p, q, m, s) = (2, 1, 2, 0)$. The initial condition has the precise form

$$a(x, 0) = a_c \left[1 + 0.02 \cos \left(\frac{\pi x}{\varepsilon} \right) e^{-x^2/(2\varepsilon)} \right], \quad h(x, 0) = h_c. \quad (5.6)$$

We plot the initial condition in Fig. 14(a). We then solve (1.1) numerically using the moving-mesh method of §2. Since very similar results are obtained from the NAG library routine D03PCF, we only display the moving-mesh results.

For this parameter set, pulse-splitting does indeed occur. In Fig. 14(b) we plot the trajectories of the center of the spike as a function of time. The spike at the origin splits into two spikes at

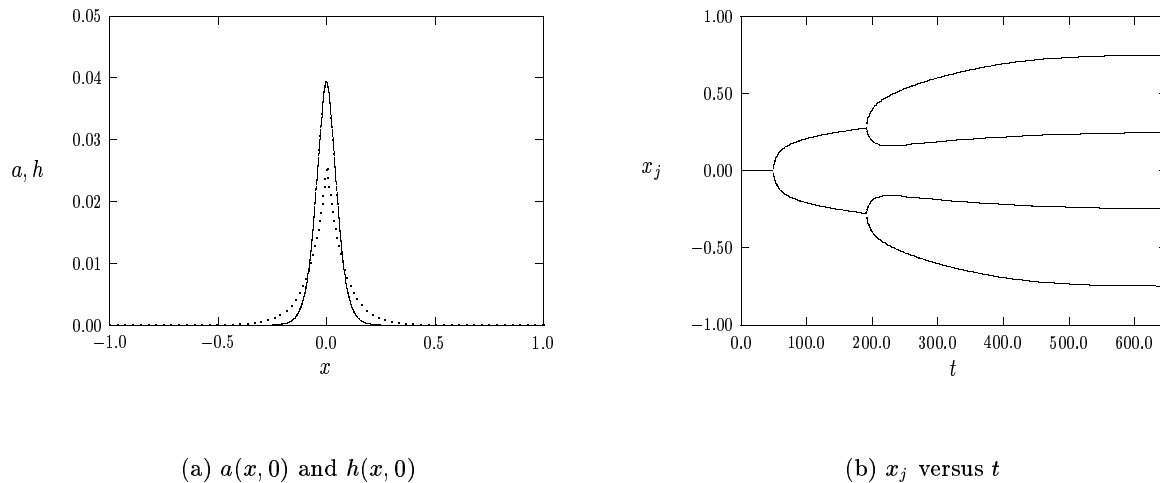
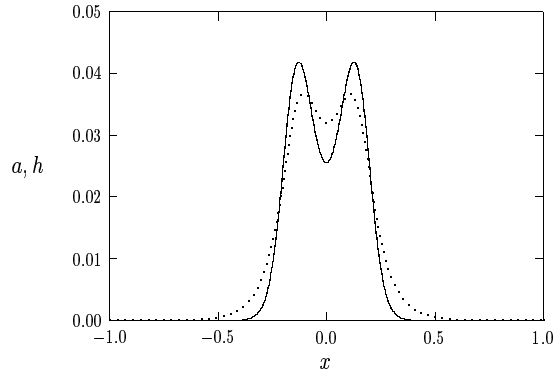


Figure 14: In the leftmost figure we plot the initial condition for a (solid curve) and for h (dashed curve). In the rightmost figure we plot the resulting spike locations versus time. The parameter values are $(p, q, m, s) = (2, 1, 2, 0)$, $\tau = 0.05$, $\varepsilon = 0.03$, and $D = 0.006$.

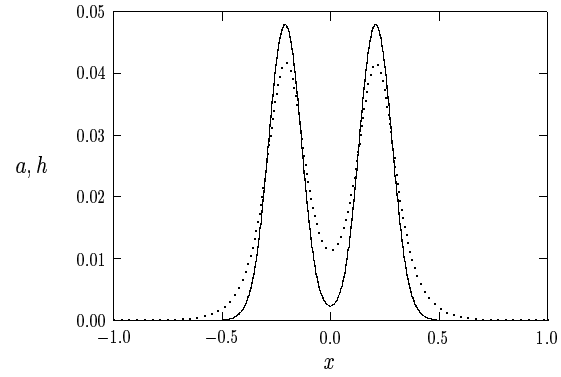
around $t = 49.5$, and a further splitting occurs at approximately $t = 191.5$. In Fig. 15(a) we plot the solution at $t = 60.5$ just after the first splitting event. In Fig. 15(b) we plot the solution at $t = 100.5$. In Fig. 16(a) we plot the solution at $t = 200.5$ just after the second splitting event. The solution at $t = 350.5$ is shown in Fig. 16(b). In Fig. 17, where $t = 1000$, the solution has essentially reached an equilibrium. This equilibrium solution more closely resembles a sinusoidal pattern for a and h rather than a sequence of spikes. The existence and stability of these large amplitude sinusoidal waves is an open problem.

The question of predicting how many splitting events will occur is presumably very difficult and depends on the parameter values. Heuristically, if ε is very small, spikes may become very well-separated after a splitting event provided that they have not reached the end of the domain. Spikes that are isolated at any time will have a tendency to split if D is below the critical value $\varepsilon^2 D_c$. The details of this mechanism, which we will not explore here, may be similar to that in the Gray-Scott model.

We have performed similar pulse-splitting experiments with other parameter values and exponent sets to test the predictions of (5.3). Pulse-splitting does indeed seem to occur when $D < \varepsilon^2 D_c$.

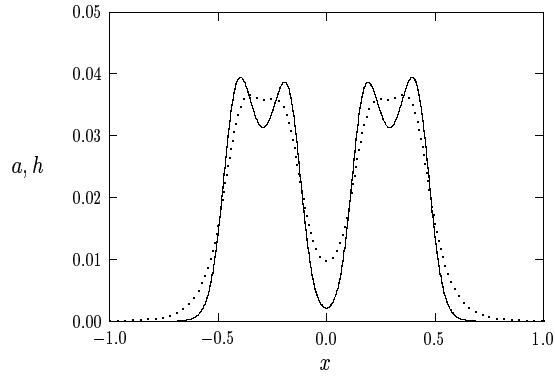


(a) a and h at $t = 60.5$

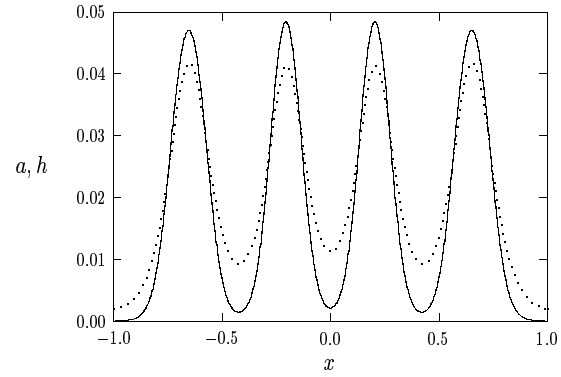


(b) a and h at $t = 100.5$

Figure 15: Plots of a (solid curve) and h (dashed curve) at two different times. The parameter values are $(p, q, m, s) = (2, 1, 2, 0)$, $\tau = 0.05$, $\varepsilon = 0.03$, and $D = 0.006$.



(a) a and h at $t = 200.5$



(b) a and h at $t = 350.5$

Figure 16: Plots of a (solid curve) and h (dashed curve) at two different times. The parameter values are $(p, q, m, s) = (2, 1, 2, 0)$, $\tau = 0.05$, $\varepsilon = 0.03$, and $D = 0.006$.

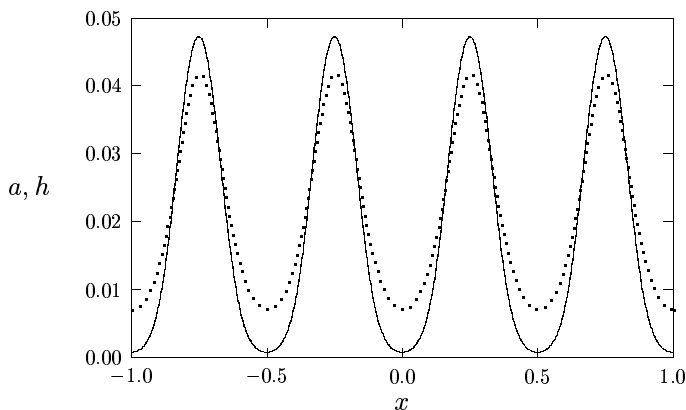


Figure 17: Plot of a (solid curve) and h (dashed curve) at $t = 1000$. This is very close to the resulting equilibrium solution. The parameter values are $(p, q, m, s) = (2, 1, 2, 0)$, $\tau = 0.05$, $\varepsilon = 0.03$, and $D = 0.006$.

6 A Generalized Gierer-Meinhardt Model

There are many activator-inhibitor models that involve coupling the basic GM model (1.1) to other differential equations that represent auxiliary chemical concentrations. In this section we consider one such extension of (1.1) that has been used in [16] to model sea-shell patterns. The generalized GM model considered in §6.2 of [16] is the following system for $a = a(x, t)$, $h = h(x, t)$, and $c = c(t)$:

$$a_t = \varepsilon^2 a_{xx} - a + \frac{a^p}{h^q}, \quad -1 < x < 1, \quad t > 0, \quad (6.1a)$$

$$\tau h_t = D h_{xx} - \mu h + \varepsilon^{-1} \frac{a^m}{h^s}, \quad -1 < x < 1, \quad t > 0, \quad (6.1b)$$

$$c_t = \kappa_c \left[\int_{-1}^1 a(x, t) dx - c \right], \quad (6.1c)$$

$$a_x(\pm 1, t) = h_x(\pm 1, t) = 0, \quad (6.1d)$$

$$a(x, 0) = a_0(x), \quad h(x, 0) = h_0(x), \quad c(0) = c_0. \quad (6.1e)$$

Here $\varepsilon \ll 1$, $\kappa_c > 0$, and $D > 0$ are constants. The exponents (p, q, m, s) are again assumed to satisfy (1.2). Here c represents the concentration of a hormone-like substance (see [16]). The coupling between h and c arises from the dependence of μ on c . From p. 94 of [16] it has the form

$$\mu = \eta/c, \quad (6.2)$$

where $\eta > 0$ is a constant.

Since the solution to this problem will again have spikes that move across the domain, we employ a moving-mesh numerical method similar to that described in §2. The semi-discrete equation for the approximation of a and h is the same as in (2.3). Using the trapezoidal rule, the approximate solution $C(t)$ for (6.1c) is required to satisfy the following semi-discrete equation, for $i = 0, \dots, N$, $t > 0$:

$$C(t)_t = \kappa_c \sum_{i=0}^{N-1} \frac{[A(t)_{i+1} + A(t)_i]}{2} (x_{i+1} - x_i) - \kappa_c C(t), \quad \text{with } C(0) = c_0. \quad (6.3)$$

The numerical procedure is as follows. Using the same monitor function as in §2, we first generate the initial mesh at $t = 0$. Then, once the approximate solution $\{A_i, H_i\}_0^n$ on the adaptive moving-mesh is known at $t = t_n > 0$, the activator concentration is computed at $t = t_{n+1}$ by means of an explicit fourth-order Runge Kutta method on the mesh $\{x(t_n)_i\}_0^N$. We then generate the adaptive moving-mesh at the next time step by solving the linearized system (2.7) with $M_{i+1/2}$ and $M_{i-1/2}$ computed by the value of $A(t_n)$. We then map the activator concentration $A(t_{n+1})$, $H(t_n)$ on the previous mesh to the current mesh by a first order linear interpolation. Next, we calculate the hormone and inhibitor concentration $C(t_{n+1})$, $H(t_{n+1})$ on the current mesh in terms of the known $A(t_{n+1})$. The computational results shown below are done using this method. These numerical results have been verified by comparing them with corresponding results computed using the routine D03PCF of the NAG library [18].

There is no quantitative analysis of (6.1) in [16]. However, it is indicated on p. 94 of [16] that the stability of the system should depend upon c through the inhibitor decay rate μ , and that pulse-splitting behavior should be possible. Our goal here is to illustrate a few of the different possibilities, and to give some quantitative estimates on the parameter ranges where different behaviors are observed.

The key parameters in the experiments below are η and κ_c . In each of our experiments, we have taken $D = 1.0$, $\varepsilon = 0.03$, $\tau = 0.5$, and the exponent set $(p, q, m, s) = (2, 1, 2, 0)$. In each case, the initial condition for a has three peaks and is given by

$$a_0(x) = 0.19 \operatorname{sech}^2 [\varepsilon^{-1}(x - 0.6)] + 0.19 \operatorname{sech}^2 [\varepsilon^{-1}(x + 0.6)] + 0.17 \operatorname{sech}^2 [\varepsilon^{-1}x]. \quad (6.4)$$

The initial condition for c is $c_0 = 0.01$, while the initial condition $h_0(x)$ is the solution to (6.1b) with $\tau = 0$, $a = a_0(x)$, and $c = c_0$. The initial condition for a is plotted in Fig. 18.

We first calculate an equilibrium k -spike solution $a_e(x)$, $h_e(x)$, and c_e , to (6.1) for $\varepsilon \ll 1$. From proposition 1 of [12], we have

$$a_e \sim H \sum_{j=1}^k w [\varepsilon^{-1}(x - x_j)], \quad H \sim 2\sqrt{\mu D} \tanh \left(\frac{1}{k} \sqrt{\frac{\mu}{D}} \right) \left(\int_{-\infty}^{\infty} [w(y)]^2 dy \right)^{-1}, \quad (6.5)$$

where $w(y) = \frac{3}{2} \operatorname{sech}^2(y/2)$ and $x_j = -1 + (2j - 1)/k$ for $j = 1, \dots, k$. In terms of H , we have

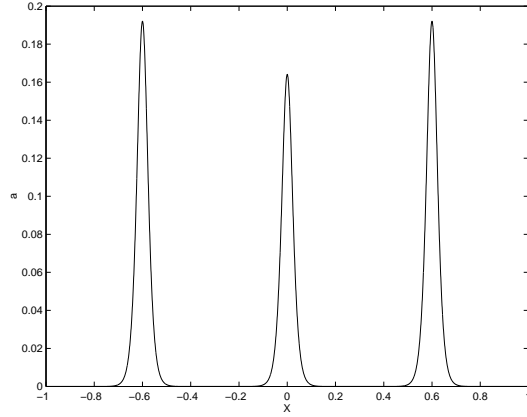


Figure 18: The initial condition $a(x, 0)$.

$h_e(x_j) = H$. In (6.5), $\mu = \eta/c_e$, where c_e satisfies

$$c_e = \int_{-1}^1 a_e(x, t) dx \sim \varepsilon k H \int_{-\infty}^{\infty} w(y) dy. \quad (6.6)$$

Substituting H from (6.5) into (6.6), and evaluating the two integrals, we obtain a transcendental equation for c_e given by

$$c_e = 2\varepsilon k \sqrt{\frac{\eta D}{c_e}} \tanh\left(\frac{1}{k} \sqrt{\frac{\eta}{c_e D}}\right). \quad (6.7)$$

It is easy to see that this equation has exactly one root for c_e . It is convenient to introduce a new variable β by $\beta = \sqrt{\mu}/k$, where $c_e = \eta/\mu$. In terms of β , when $D = 1$, then (6.7) becomes

$$\beta^3 \tanh \beta = \frac{\eta}{2\varepsilon k^4}, \quad \mu = \beta^2 k^2, \quad (6.8)$$

where $\varepsilon = 0.03$.

We now recall some previous stability results for (6.1) when μ is constant and $\tau = 0$. From proposition 11 of [12] we conclude that, when $\tau = 0$ and μ is constant, a k -spike equilibrium solution with $k \geq 2$ is stable if and only if $D/\mu < k^{-2} [\log(1 + \sqrt{2})]^{-2}$. Since $D = 1$, we can use (6.8) to predict that a k -spike equilibrium solution to (6.1) with $k \geq 2$ will be stable for $\tau = 0$, when

$$\beta > \log [1 + \sqrt{2}] = 0.881. \quad (6.9)$$

In addition, if a k -spike equilibrium solution with $k \geq 2$ is unstable for $\tau = 0$ it will be unstable for $\tau > 0$ (cf. [31]). However, if a k -spike equilibrium solution is stable for $\tau = 0$ it does not mean that

we will have stability when $\tau > 0$. For multi-spike solutions, the critical bounds on D for $\tau > 0$ are as yet unknown. A one-spike equilibrium solution is stable for $\tau = 0$ for any $D > 0$. In §4 we determined the stability of a one-spike solution for (1.1) when $\tau > 0$. When μ is constant, we can introduce $\tilde{D} = D/\mu$ and $\tilde{\tau} = \tau/\mu$, and make a change of variables for a and h , as in Appendix A, to map (6.1a), (6.1b) to (1.1a) and (1.1b). This allows us to apply the stability conclusions of §4. We predict that a one-spike solution for (6.1) will be stable when

$$\tau < \mu\tau_0. \quad (6.10)$$

Here τ_0 is the value on the vertical axis in Fig. 4(a) of §4 at the value $1/\mu$ along the horizontal axis. If (6.10) is satisfied, then there will be no oscillatory instability for a one-spike equilibrium solution.

Finally, from §5, we predict that pulse-splitting should occur when $D/\mu < 7.171\varepsilon^2$, where $D = 1$. In terms of η , this condition becomes

$$\eta > \frac{c}{7.171\varepsilon^2}. \quad (6.11)$$

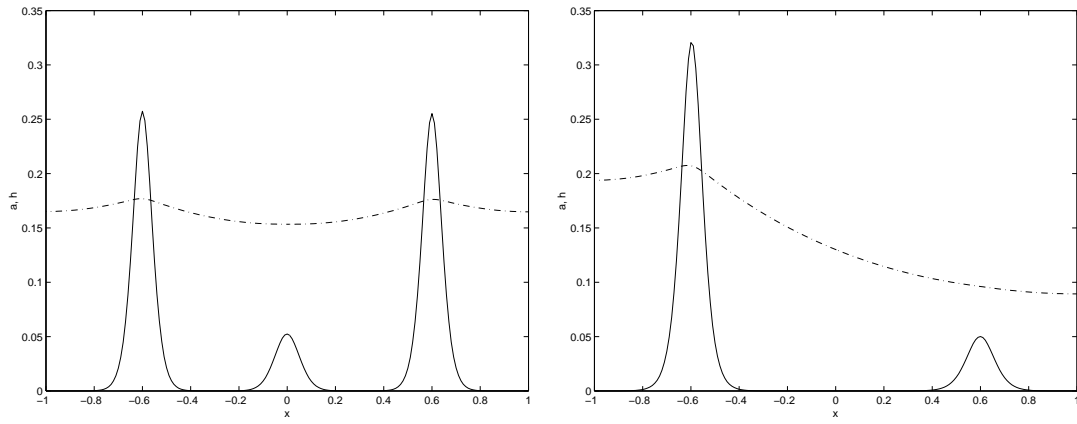
Pulse-splitting can occur quickly in time for (6.1) if κ_c is very large. When $\kappa_c \gg 1$, then c relaxes quickly to $c \approx \int_{-1}^1 a(x, 0) dx$. Using $a(x, 0)$ in (6.4), we calculate $c \sim 1.1\varepsilon$. Using this value in (6.11), we predict that pulse-splitting will occur quickly in time for $\varepsilon = 0.03$ when

$$\eta > 0.1534\varepsilon^{-1} \approx 4.755. \quad (6.12)$$

Qualitatively, this scenario suggests that as η is increased with $\kappa_c = O(1)$, then more spikes can become stable. However, if both κ_c and η are very large, then pulse-splitting can occur. The system (6.1) is very complicated and certainly difficult to analyze in precise terms since, as we have seen from §4, we can also have oscillatory instabilities that suddenly arise during the evolution of spikes when τ is large enough. For the experiments below, the effective value of τ is small and so oscillatory instabilities do not occur. Therefore, the estimates given above do provide some rough guidelines on the range of behaviors seen.

Experiment 1: We take the parameter values $\kappa_c = 0.1$ and $\eta = 1.0$. From (6.8) we calculate $\beta = 0.698$ when $k = 3$. Hence, from (6.9) we expect that a 3-spike equilibrium solution will be unstable when $\tau = 0$, and, thus, unstable when $\tau > 0$. For $k = 1$, we calculate from (6.8) that $\beta = 2.5645$ and $\mu = \beta^2 \approx 6.58$. Then, from Fig. 4(a) of §4 we calculate $\tau_0 \approx 2.73$ when $D = 1/\mu \approx 0.152$ along the x-axis of Fig. 4(a). Thus, for $\tau = 0.5$, the inequality (6.10) is satisfied and a one-spike solution is stable. For $k = 2$, we calculate $\beta = 1.093$ from (6.8). Thus, from (6.9), we have that a two-spike equilibrium solution is stable when $\tau = 0$. However, as mentioned above, we can make no conclusion about the stability of this solution when $\tau > 0$.

In Fig. 19–20 we show that an initial three-bump solution undergoes a series of transitions eventually producing a one-spike solution. The remaining spike then moves slowly towards the midpoint of the domain.



(a) a and h at $t = 2.0$

(b) a and h at $t = 15.0$

Figure 19: Plots of a (solid curve) and h (dashed curve) for Experiment 1 at different times.

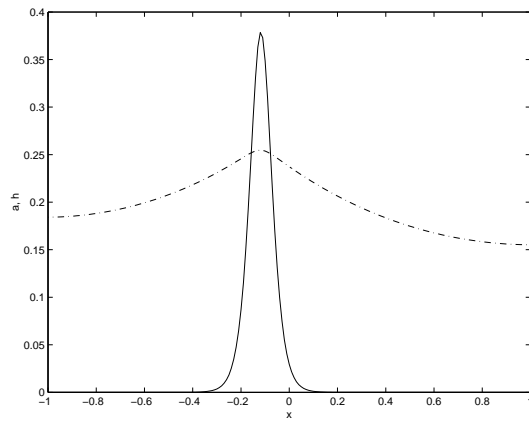


Figure 20: Plot of a (solid curve) and h (dashed curve) for Experiment 1 at $t = 2000$.

Experiment 2: In this example we show that, depending on the values of η and k_c , an initial condition with three peaks can be stabilized to an equilibrium solution with either two or three spikes. In Fig. 21(a) we exhibit the resulting two-spike solution when $k_c = 100$, $\eta = 2.0$ and $t = 200$. In Fig. 21(b) we exhibit the resulting three-spike solution for $k_c = 20$, $\eta = 4.3$, and $t = 500$. In each case, the numerics indicates that we have reached a stable equilibria.

When $\eta = 2.0$, we calculate from (6.8) that $\beta = 1.337$ when $k = 2$, and $\beta = 0.843$ when $k = 3$. Thus, from (6.9) we conclude that a two-spike equilibrium solution is stable when $\tau = 0$, but that a three-spike equilibrium solution is unstable when $\tau = 0$ and also $\tau > 0$. We can offer no conclusion on the stability of the two-spike equilibrium solution when $\tau = 0.5$. For a one-spike solution, we calculate $\beta = 3.221$ from (6.8). We can again estimate the critical value of τ for a Hopf bifurcation, to conclude that a one-spike solution is stable when $\tau = 0.5$. Finally, when $\eta = 4.3$, we calculate $\beta = 1.022$. Thus, a three-spike equilibrium solution is stable when $\tau = 0$. The numerical results shown in Fig. 21(b) indicate that it must be stable when $\tau = 0.5$.

Although κ_c is large in each of these examples, the predicted threshold (6.12) for pulse-splitting is not satisfied. Pulse-splitting behavior was not found in these examples.

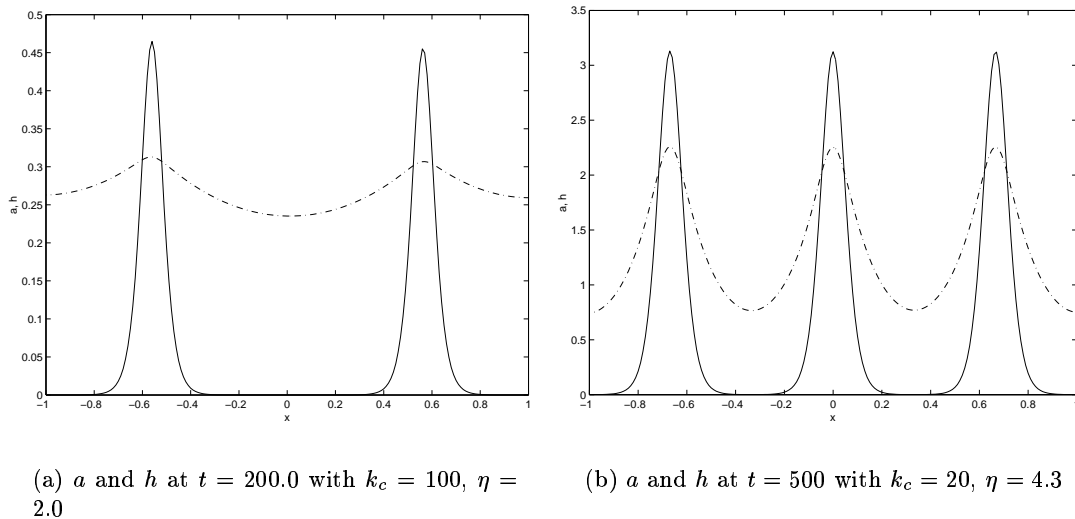


Figure 21: Plots of a (solid curve) and h (dashed curve) for Experiment 2. For both plots we have, numerically, reached an equilibrium.

Experiment 3: Finally, we show that pulse-splitting behavior can occur when κ_c is very large and the criterion (6.12) is satisfied. We take $k_c = 10000$ and $\eta = 100$. In Fig. 22, we exhibit a pulse-splitting behavior when $t = 70$. The splitting behavior is complete when $t = 100$ as shown in Fig. 23(a). Finally, in Fig. 23(b) we show that the pattern reaches an equilibrium solution,

resembling a large amplitude sinusoidal wave with five maxima, when $t = 500$.

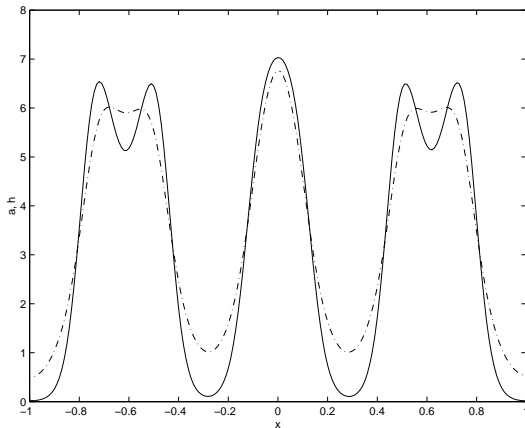


Figure 22: Plot of a (solid curve) and h (dashed curve) for Experiment 3 at $t = 70$ showing the pulse-splitting behavior.

Acknowledgements

J. W. thanks the support of RGC of Hong Kong and a direct grant from CUHK. T. T. thanks the supports provided by RGC of Hong Kong and FRG of the Hong Kong Baptist University. M. J. W. thanks NSERC and the IMS of the Chinese University of Hong Kong, where this paper was written.

A Nondimensionalizing the GM and Schnakenburg Models

The dimensional Gierer-Meinhardt model is

$$A_T = D_1 A_{yy} - \alpha A + \beta \frac{A^p}{H^q}, \quad (\text{A.1a})$$

$$H_T = D_2 H_{yy} - \xi H + \sigma \frac{A^m}{H^s}, \quad (\text{A.1b})$$

where α , β , ξ , and σ , are positive constants. The exponents (p, q, m, s) satisfy (1.2). We assume that D_2/D_1 is large, and so we introduce a small parameter ε by

$$\frac{D_2}{D_1} = \varepsilon^{-2} K_0, \quad (\text{A.2})$$

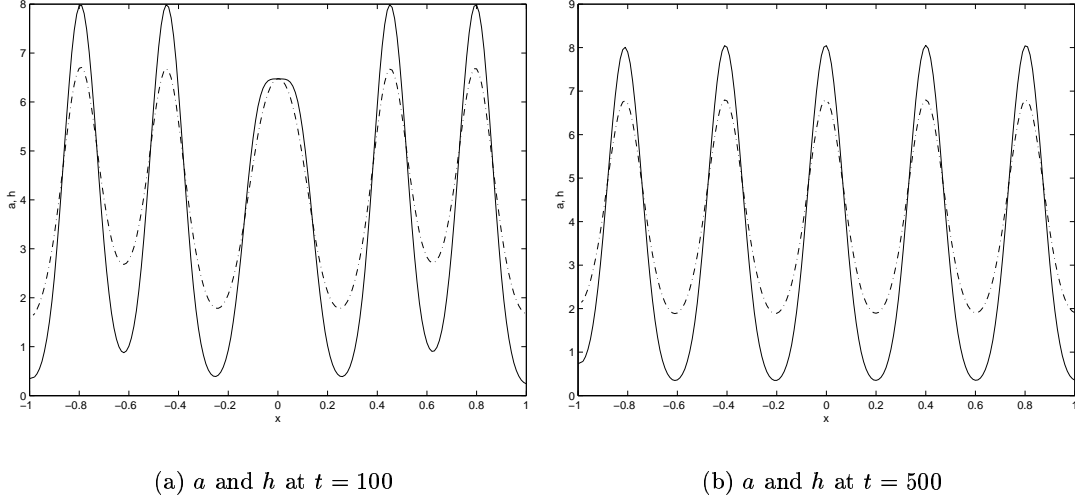


Figure 23: Plots of a (solid curve) and h (dashed curve) for Experiment 3 at two different times.

where $K_0 > 0$ is $O(1)$ as $\varepsilon \rightarrow 0$. In this limit, (A.1) supports spike solutions that are localized in A . We introduce dimensionless variables a , h , t and x , by

$$T = \omega t, \quad x = y/L, \quad A = \varepsilon^{-\nu_a} a_0 a, \quad H = \varepsilon^{-\nu_h} h_0 h, \quad (\text{A.3})$$

where a_0 and h_0 are constants. Substituting (A.3) into (A.1), we get

$$\frac{1}{\omega} a_t = \frac{D_1}{L^2} a_{xx} - \alpha a + \beta \varepsilon^{\nu_a(1-p) + \nu_h q} \left(\frac{a_0^{p-1}}{h_0^q} \right) \frac{a^p}{h^q}, \quad (\text{A.4a})$$

$$\frac{1}{\omega} h_t = \frac{D_2}{L^2} h_{xx} - \xi h + \sigma \varepsilon^{-\nu_a m + \nu_h(1+s)} \left(\frac{a_0^m}{h_0^{s+1}} \right) \frac{a^m}{h^s}. \quad (\text{A.4b})$$

To ensure that the amplitude of a spike is $O(1)$ as $\varepsilon \rightarrow 0$, we must make the coefficients of a^p/h^q and a^m/h^s be $O(1)$ and $O(\varepsilon^{-1})$ as $\varepsilon \rightarrow 0$, respectively. This condition yields that

$$\nu_a = \frac{q}{p-1} \zeta^{-1}, \quad \nu_h = \zeta^{-1}, \quad (\text{A.5})$$

where ζ was defined in (1.2). To eliminate as many parameters as possible in (A.4), we choose ω and L by $\omega = 1/\alpha$ and $L^2 = D_1 \varepsilon^{-2}/\alpha$. The constants a_0 and h_0 are taken to be

$$h_0 = \left[\frac{\xi}{\sigma} \left(\frac{\beta}{\alpha} \right)^{\frac{m}{p-1}} \right]^{\frac{1}{\zeta}}, \quad a_0 = \left(\frac{\alpha}{\beta} \right)^{\frac{1}{p-1}} \left[\frac{\xi}{\sigma} \left(\frac{\beta}{\alpha} \right)^{\frac{m}{p-1}} \right]^{\frac{q}{(p-1)\zeta}}. \quad (\text{A.6})$$

Then, (A.4) becomes

$$a_t = \varepsilon^2 a_{xx} - a + \frac{a^p}{h^q}, \quad (\text{A.7a})$$

$$\tau h_t = \tau \varepsilon^2 \left(\frac{D_2}{D_1} \right) h_{xx} - h + \varepsilon^{-1} \frac{a^m}{h^s}. \quad (\text{A.7b})$$

Finally, substituting (A.2) for D_2/D_1 into (A.7b), we obtain the dimensionless system (1.1) where τ and D in (1.1) are defined by

$$\tau \equiv \alpha/\xi \quad D \equiv \tau K_0. \quad (\text{A.8})$$

The dimensional Schnakenburg model is

$$U_T = D_1 U_{yy} - a_1 U + a_2 U^2 V, \quad (\text{A.9a})$$

$$V_T = D_2 V_{yy} + b_1 - b_2 U^2 V, \quad (\text{A.9b})$$

where a_1 , a_2 , b_1 , and b_2 are positive constants. We assume that D_2/D_1 is large, and so we introduce a small parameter ε by

$$\frac{D_2}{D_1} = \varepsilon^{-3} K_0, \quad (\text{A.10})$$

where $K_0 > 0$ is $O(1)$ as $\varepsilon \rightarrow 0$. Notice here that the scaling is different than in (A.2) for the GM model. We introduce dimensionless variables u , v , t and x , by

$$T = \omega t, \quad x = y/L, \quad U = \varepsilon^{-1} u_0 u, \quad V = \varepsilon v_0 v, \quad (\text{A.11})$$

where u_0 and v_0 are constants. Substituting (A.11) into (A.9), we get

$$\frac{1}{\omega} u_t = \frac{D_1}{L^2} u_{xx} - a_1 u + a_2 (u_0 v_0) u^2 v, \quad (\text{A.12a})$$

$$\frac{\varepsilon v_0}{2\omega b_1} v_t = \frac{\varepsilon D_2 v_0}{2b_1 L^2} v_{xx} + \frac{1}{2} - \frac{b_2}{2b_1 \varepsilon} (u_0^2 v_0) u^2 v. \quad (\text{A.12b})$$

To eliminate as many parameters as possible in (A.12), we choose ω and L by $\omega = 1/a_1$ and $L^2 = D_1 \varepsilon^{-2}/a_1$. We also take $u_0 v_0 = a_1/a_2$. With this scaling, (A.12) transforms to

$$u_t = \varepsilon^2 u_{xx} - u + u^2 v, \quad (\text{A.13a})$$

$$\frac{\varepsilon a_1 v_0}{2b_1} v_t = \frac{a_1 v_0 D_2 \varepsilon^3}{2b_1 D_1} v_{xx} + \frac{1}{2} - \frac{b_2}{2b_1 v_0} \left(\frac{a_1}{a_2} \right)^2 \varepsilon^{-1} u^2 v. \quad (\text{A.13b})$$

We then choose v_0 as

$$v_0 = b \equiv \frac{b_2}{2b_1} \left(\frac{a_1}{a_2} \right)^2. \quad (\text{A.14})$$

Finally, substituting (A.10) for D_2/D_1 into (A.13b), we obtain the dimensionless system

$$u_t = \varepsilon^2 u_{xx} - u + u^2 v, \quad (\text{A.15a})$$

$$\varepsilon \tau_0 v_t = D v_{xx} + \frac{1}{2} - \varepsilon^{-1} u^2 v. \quad (\text{A.15b})$$

Here τ_0 and D are defined by

$$\tau_0 \equiv \left(\frac{a_1}{2b_1} \right) b, \quad D \equiv \tau_0 K_0, \quad (\text{A.16})$$

with b given in (A.14).

Thus, when the coefficients a_1 , a_2 , b_1 , and b_2 , in (A.9) are $O(1)$ as $\varepsilon \rightarrow 0$, the natural scaling for a spike solution to the Schnakenburg model (A.9) is such that the v component has a slow time-dependence. This is quite different from the GM nondimensionalization leading to (1.1). To incorporate the effect of the τ term in (1.3b), we consider a related distinguished limit where $\tau_0 = O(\varepsilon^{-1})$ in (A.15b) and $D = O(1)$ as $\varepsilon \rightarrow 0$. From (A.16) and (A.10), this implies that $K_0 = O(\varepsilon)$ and $D_2/D_1 = O(\varepsilon^{-2})$ as $\varepsilon \rightarrow 0$. When $\tau_0 = O(\varepsilon^{-1})$, we obtain the system (1.3), where τ in (1.3b) is given by $\tau \equiv \varepsilon \tau_0$.

References

- [1] U. Ascher, R. Christiansen, R. Russell, *Collocation Software for Boundary Value ODE's*, Math. Comp., **33**, (1979), pp. 659-679.
- [2] J. U. Brackbill, J. S. Saltzman, *Adaptive Zoning for Singular Problems in Two Dimensions*, J. Comput. Phys., **46**, (1982), pp. 342-368.
- [3] J. G. Blom, P. A. Zegeling, *Algorithm 731: A Moving-Grid Interface for Systems of One-Dimensional Time-Dependent Partial Differential Equations*, Trans. Math. Software **20**, No. 2, (1994), pp. 194-214.
- [4] C. De Boor, *Good Approximation by Splines with Variable Knots II*, in Springer Lecture Notes Series 363, Springer-Verlag, Berlin, (1973).
- [5] A. Doelman, T. J. Kaper, P. Zegeling, *Pattern Formation in the One-Dimensional Gray-Scott Model*, Nonlinearity, **10**, (1997), pp. 523-563.
- [6] A. Doelman, R. A. Gardner, T. J. Kaper, *Stability Analysis of Singular Patterns in the 1D Gray-Scott Model: A Matched Asymptotics Approach*, Physica D, **122**, (1998), pp. 1-36.
- [7] A. Doelman, R. A. Gardner, T. Kaper, *A Stability Index Analysis of 1-D Patterns of the Gray Scott Model*, Memoirs of the AMS, **155**, No. 737, (2002).

- [8] A. Doelman, H. van der Ploeg, *Homoclinic Stripe Patterns*, preprint, Univ. of Amsterdam, (2001).
- [9] A. Gierer, H. Meinhardt, *A Theory of Biological Pattern Formation*, *Kybernetik*, **12**, (1972), pp. 30–39.
- [10] L. Harrison, D. Holloway, *Order and Localization in Reaction-Diffusion Pattern*, *Physica A*, **222**, (1995), pp. 210-233.
- [11] D. Iron, M. J. Ward, *The Dynamics of Multi-Spike Solutions to the One-Dimensional Gierer-Meinhardt Model*, to appear, *SIAM J. Appl. Math.*, (2002).
- [12] D. Iron, M. J. Ward, J. Wei, *The Stability of Spike Solutions to the One-Dimensional Gierer-Meinhardt Model*, *Physica D*, **150**, No. 1-2, (2001), pp. 25-62.
- [13] D. Iron, J. Wei, M. Winter, *Stability Analysis of Turing Patterns Generated by the Schnakenberg Model*, submitted, *J. Math. Biology*, (2001).
- [14] R. Li, T. Tang, and P. W. Zhang, *Moving Mesh Methods in Multiple Dimensions Based on Harmonic Maps*, *J. Comput. Phys.*, **170**, (2001), pp. 562-588.
- [15] H. Meinhardt, *Models of Biological Pattern Formation*, Academic Press, London (1982).
- [16] H. Meinhardt, *The Algorithmic Beauty of Sea Shells*, Springer-Verlag, Berlin, (1995).
- [17] C. Muratov, Osipov *Traveling Spike Auto-Solitons in the Gray-Scott Model*, *Physica D*, **155**, No. 1-2, (2001), pp. 112-131.
- [18] NAG Fortran library Mark 17, routine D03PCF, Numerical Algorithms Group Ltd., Oxford, United Kingdom (1995).
- [19] W. Ni, *Diffusion, Cross-Diffusion, and Their Spike-Layer Steady-States*, *Notices of the AMS*, Vol. **45**, No. 1, (1998), pp. 9-18.
- [20] W. Ni, I. Takagi, E. Yanagida, *Stability Analysis of Point-Condensation Solutions to a Reaction-Diffusion System Proposed by Gierer and Meinhardt*, to appear, *Tohoku Math J.*, (2002).
- [21] Y. Nishiura, private communication.
- [22] Y. Nishiura, D. Ueyama, *A Skeleton Structure of Self-Replicating Dynamics*, *Physica D*, **130**, (1999), pp. 73-104.
- [23] Y. Nishiura, D. Ueyama, *Spatio-Temporal Chaos for the Gray-Scott Model*, *Physica D*, **150**, (2001), pp. 137-162.

- [24] W. Q. Ren, X. P. Wang, *An Iterative Grid Redistribution Method for Singular Problems in Multiple Dimensions*, J. Comput. Phys., **159**, (2000), pp.246–273.
- [25] W. N. Reynolds, S. Ponce-Dawson, J. E. Pearson, *Self-Replicating Spots in Reaction-Diffusion Systems*, Phys. Rev. E, **56**, (1997), pp. 185-198.
- [26] J. Schnakenberg, *Simple Chemical Reaction Systems with Limit Cycle Behavior*, J. Theoret. Biology, **81**, (1979), p. 389-400.
- [27] A. Turing, *The Chemical Basis of Morphogenesis*, Phil. Trans. Roy. Soc. B, **327**, (1952), pp. 37-72.
- [28] M. J. Ward, J. Wei, *Asymmetric Spike Patterns for the One-Dimensional Gierer-Meinhardt Model*, to appear, Europ. J. Appl. Math., (2002).
- [29] M. J. Ward, J. Wei, *The Existence and Stability of Asymmetric Spike Patterns for the Schnakenburg Model*, to appear, Studies in Appl. Math., (2002).
- [30] M. J. Ward, J. Wei, *Hopf Bifurcation of Spike Solutions for the Shadow Gierer-Meinhardt Model*, submitted, Europ. J. Appl. Math., (2002).
- [31] M. J. Ward, J. Wei, *Hopf Bifurcations and Oscillatory Instabilities of Spike Solutions for the One-Dimensional Gierer-Meinhardt Model*, preprint.
- [32] J. Wei, *On Single Interior Spike Solutions for the Gierer-Meinhardt System: Uniqueness and Stability Estimates*, Europ. J. Appl. Math., Vol. **10**, No. 4, (1999), pp. 353-378.
- [33] J. Wei, M. Winter, *The Gierer-Meinhardt System: Existence and Stability of N-Peaked Solutions*, submitted, Trans. American Math Society, (2001).
- [34] A. B. White, *On Selection of Equidistribution Meshes for Two-Point Boundary Value Problems*, SIAM J. Numer. Anal., **16**, (1979), pp. 472-502.